Contrib Mineral Petrol (2005) 150: 335–353
DOI 10.1007/s00410-005-0026-7

ORIGINAL PAPER

Dmitri A. Ionov · Ingrid Chanefo · Jean-Louis Bodinier

Origin of Fe-rich lherzolites and wehrlites from Tok, SE Siberia by reactive melt percolation in refractory mantle peridotites

Received: 23 March 2005 / Accepted: 2 August 2005 / Published online: 3 September 2005

Abstract Lherzolite–wehrlite (LW) series xenoliths from the quaternary Tok volcanic field in the southeastern Siberian craton are distinguished from the more common lherzolite–harzburgite (LH) series by (a) low Mg numbers (0.84–0.89) at high modal olivine (66–84%) and (b) widespread replacement of orthopyroxene (0–12%) and spinel by clinopyroxene (7–22%). The LW series peridotites are typically enriched in Ca, Fe, Mn and Ti, and depleted in Si, Ni and Cr relative to refractory LH series rocks (Mg number ≥0.89), which are metasomatised partial melting residues. Numerical modelling of Fe–Mg solid/liquid exchange during melt percolation demonstrates that LW series rocks can form by reaction of host refractory peridotites with evolved (Mg numbers 0.6–0.7), silica-undersaturated silicate melts at high melt/rock ratios, which replace orthopyroxene with clinopyroxene and decrease Mg numbers. This process is most likely related to underplating and fractionation of basaltic magma in the shallow mantle, which also produced olivine–clinopyroxene cumulates found among the Tok xenoliths.

Keywords Siberia · Lithospheric mantle · Peridotite · Wehrlite · Reactive melt percolation

Communicated by J. Hoefs

D. A. Ionov (✉)
Abteilung Geochemie, Max-Planck-Institut für Chemie, Postfach 3060, 55020 Mainz, Germany
E-mail: ionov@mpch-mainz.mpg.de
Tel.: +49-6131-305281
Fax: +49-6131-371051

I. Chanefo · J.-L. Bodinier · D. A. Ionov
Laboratoire de Tectonophysique, UMR 5568 CNRS, ISTEEM, Université Montpellier 2, case 049, 34095 Montpellier, Cedex 05, France

Introduction

Peridotite xenoliths brought up to the surface by volcanic eruptions are direct samples of the lithospheric mantle. The most common rock types among the xenoliths (and hence in the lithospheric mantle) are lherzolites and harzburgites with Mg numbers ≥0.89 [Mg# = $Mg/(Mg+Fe)_{at}$]. Such rocks are generally considered as residues after different degrees of melt extraction from fertile mantle based on various petrological data and comparisons with experimental results (Pearson et al. 2003; Walter 2003). Although some of those peridotites are metasomatised (Frey and Green 1974; Menzies and Hawkesworth 1987; Pearson et al. 2003), the metasomatism normally does not significantly affect their modal and major element compositions.

Many mantle peridotite series, however, also include other rock types (mainly dunite and wehrlite) (Frey and Green 1974; Frey and Prinz 1978; Jackson and Wright 1970; Neumann et al. 2002; Peslier et al. 2002; Wilshire and Shervais 1975; Xu et al. 1996), which are not likely to be partial melting residues. In some cases, such rocks make up the majority of xenolith populations (Fodor and Galar 1997; Lee and Rudnick 1999; Tommasi et al. 2004; Xu et al. 2003). Although it is generally assumed that reaction of residual wall-rock peridotites with migrating magmatic liquids plays a major role in the origin of such peridotites, the composition of the liquids and the exact nature of the rock–melt interaction remains a matter of debate (Kelemen et al. 1992; Menzies and Hawkesworth 1987; Pearson et al. 2003). In particular, the origin of non-cumulate wehrlites and clinopyroxene-rich lherzolites has been attributed to reaction with either carbonate-rich liquids (Hauri et al. 1993; Neumann et al. 2002; Yaxley et al. 1991) or basaltic melts (Batanova et al. 1998; Godard et al. 2000; Parkinson et al. 2003; Peslier et al. 2002).

Alkali basaltic rocks in the Tokinsky Stanovik Range near the southeastern rim of the Aldan shield (Fig. 1) contain particularly abundant, large and fresh

"non-residual" peridotite xenoliths. While Kiselev et al. (1979) and Semenova et al. (1984) reported (in Russian) that the Tok suite contains mantle xenoliths of the "Al-augite" series, no geochemical data on those xenoliths have been published as yet, to the best of our knowledge, in peer-reviewed international literature. Recently, Ionov et al. (2005b) reported petrographic and chemical data for over 30 xenoliths of the "lherzolite–harzburgite" (LH) series from Tok and argued that those rocks represent partial melting residues variably affected by metasomatism. They also noted that a large number of peridotite xenoliths in their collection belong to a distinct, Fe-rich "lherzolite–wehrlite" (LW) series.

Here, we report petrographic and chemical data on the Fe-rich lherzolites and wehrlites and explore their origins. We show that the Tok suite contains a variety of rock types, which enable to relate the LW series both to their parental refractory melting residues and to evolved basaltic liquids. Importantly, we use numerical modelling of peridotite–melt reactions to argue that low Mg# and high modal clinopyroxene (Cpx) in olivine-rich mantle peridotites from the SE Siberian craton and elsewhere could be produced by reactive percolation of evolved, Fe-rich undersaturated silicate melts.

Samples and analytical procedures

Samples for this study come from the Stanovoy block of the Aldan shield in the southeastern Siberian craton (Fig. 1), which formed 2–3.6 Gy ago (Zonenshain et al. 1990). The xenoliths were collected in massive lavas (hawaiites, basanites and nephelinites) along the lower Nakit Creek near its confluence with river Tok. Geographic coordinates determined using GPS are: 55°38′38′ N, 130°06′09′ E for sampling sites 9502 and 9508, and 55°37′44′ N and 130°06′07′ E for site 9510. Rasskazov et al. (2000) reported an age interval of 0.59–0.28 Ma for volcanic rocks from the Tok volcanic field using laser Ar–Ar technique. For more information on local geology and the xenolith suite see Ionov et al. (2005b).

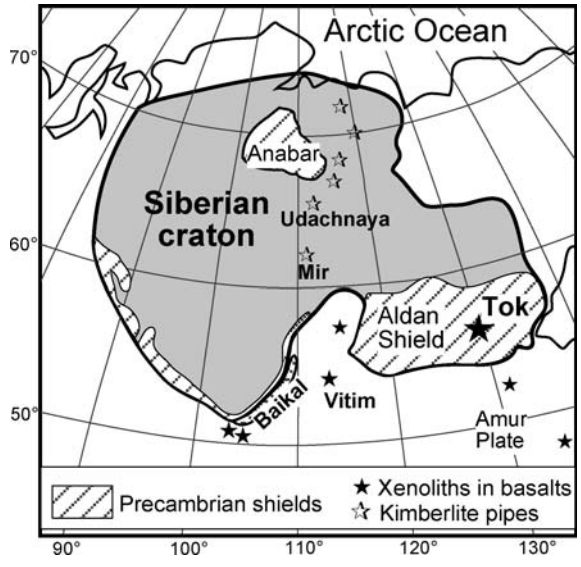

Fig. 1 A sketch map of the Siberian craton and adjacent regions (modified from Zonenshain et al. 1990)

Forty-four non-cumulate peridotite xenoliths from Tok were initially chosen for a geochemical study mainly based on their size, homogeneity, lack of secondary alteration and basaltic veins, in particular to provide clean and representative whole-rock samples. That initial sample selection did not favour any specific rock type. Twelve out of the total of 44 samples were later classified as LW series, which is the subject of this study. We also report data for one olivine–Cpx cumulate. Those xenoliths are listed in Table 1, which gives a summary of petrographic features, modal compositions, geothermometry and other essential information. Data on the other Tok xenoliths as well as detailed descriptions of sample preparation and analytical methods were reported by Ionov et al. (2005b).

Clean rock chips or slabs cut from central parts of xenoliths (weighing 115–1,070 g, Table 1) were crushed to $\leq$ 1–2 mm. Their split aliquots were ground to fine powder in agate. Nine whole-rock xenoliths and a host basalt were analysed by X-ray fluorescence (XRF) spectrometry at Franklin & Marshall College (Lancaster, USA) using procedures given by Boyd et al. (1993). Three peridotites were analysed at the University of Niigata, Japan (Takazawa et al. 2003). Several xenoliths were also analysed at the University of Mainz; reference sample JP-1 was run in the same batch as unknown and yielded values close to recommended values. The duplicate analyses done at Niigata and Mainz gave consistent results as discussed by Ionov et al. (2005b). Major oxide data from F&MC are consistent with those from Niigata and Mainz while systematic differences were found for Mn, Ni, Na and K. The F&MC data for these elements are corrected correspondingly when the data are plotted together.

Mineral compositions were determined by electron probe microbeam analysis (EPMA) at Université Montpellier 2 and Université Blaise Pascal, Clermont-Ferrand (France) on Cameca SX-100 instruments using routine techniques: 20 kV accelerating voltage, 10 nA current, 20–30 s counting times. High-precision olivine analyses were obtained on a Jeol JXA8200 instrument at MPI-Chemie, Mainz using 20 kV accelerating voltage, 20 nA current and counting times of 60–120 s. San Carlos olivine was repeatedly analysed as unknown for quality control to yield precision (reproducibility, 1σ/mean) of 0.2–0.4% for Fe and Mg, 0.04% for Mg# and 1–4% for Ni and Mn (See Ionov et al. (2005b) for more details).

Weight proportions of minerals (modal compositions) were calculated from whole-rock and mineral major element analyses by mass balance using least-squares regression.

Table 1 A summary of petrographic and other data on lherzolite–wehrlite series Tok xenoliths

Sample number	WR (g)	Rock type	Mg#	Black	Fluid inclusions	Calculated modal abundances (wt %)							T°C
			Ol	vugs		Ol	Opx	Cpx	Spl	Fs	Ap	Am,phl	Ca-opx
9502-1	539	Wehrlite	0.870	+	–	78.3	0.9	19.5	0.3	0.9	0.15		
9502-2	457	Wehrlite	0.884	+	+	79.0	4.4	13.6	0.6	2.4	0.07		909
9502-3	223	Low-opx lherzolite	0.884	+	–	79.6	5.2	11.9	0.7	2.5	0.13	am	908
9502-4	163	Wehrlite	0.880	+	+	80.3	1.0	15.4	0.6	2.6	0.19	am	
9502-10	308	Low-opx lherzolite	0.882	+	–	66.4	10.5	18.1	2.5	2.4	0.14	(phl?)	1,024
9503-2	540	Low-opx lherzolite	0.890			75.9	5.9	15.2	0.8		0.12	2.1	949
9503-22	312	Wehrlite	0.860			82.3	tr.	15.8	0.3	1.4	0.12		
9507-6	115	Wehrlite								0.9	0.10		
9508-10	1,070	Wehrlite	0.877	+	+	79.1	1.1	16.6	0.9	2.3	0.13		984
9510-1	302	Wehrlite	0.857	+	–	71.5	2.9	22.4	1.5	1.6	0.10		964
9510-3	246	Wehrlite	0.842	+	+	84.2	–	15.6	0.1		0.11		982
9510-11	420	Lherzolite	0.851	+	–	78.2	12.6	7.4	0.4	1.1	0.42		920
9508-14		Ol–cpx cumulate	0.805										

Ol, olivine; *Opx*, orthopyroxene; *Cpx*, clinopyroxene; *Spl*, spinel; *Fs*, feldspar; *Phl*, phlogopite; *Am*, amphibole; *Ap*, apatite. Petrographic features: –, absent; +, present; *tr*, traces; (phl), minerals replaced by fine-grained Fs-rich material.
Mg#, $Mg/(Mg+Fe)_{at}$. WR, weight of crushed whole-rock samples. Temperature (T) estimates are after Brey and Köhler (1990)

Three whole-rock xenoliths and one host basalt were analysed for trace elements by solution inductively coupled plasma mass-spectrometry (ICPMS) on a VG Elemental Plasma Quad II instrument at Montpellier following routine techniques established at that laboratory (Ionov et al. 1992, 2005b; Kalfoun et al. 2002).

Petrography

We distinguish, following Ionov et al. (2005b), three main rock series among spinel (Spl) peridotite xenoliths sampled at the Tok site based on microstructures, mineral proportions (Streckeisen 1976) and Mg#: LH, LW and olivine–Cpx cumulate. The subject of this study is peridotites of the LW series, which are characterised mainly by low modal orthopyroxene (Opx) and Mg# ≤ 0.89 (i.e. lower than in partial melting residues). We refer to Ionov et al. (2005b) in the following text for data on the LH series (peridotites with "normal" pyroxene abundances and Mg# ≥0.89), which are inferred to be residues of variable degrees of melt extraction from a fertile source.

The LW series comprises olivine-rich (66–84 wt.% Ol; Table 1) peridotites, which either contain no Opx or show widespread replacement of Opx by Cpx (Fig. 2a–d). The LW series can be subdivided into three groups in terms of Opx abundances and Opx–Cpx relationships. (1) Low-Opx (5–13%) lherzolites show different stages of Opx replacement, from nearly intact Opx grains with rare Cpx at rims to Opx embayed with Cpx to resorbed Opx relics inside newly formed Cpx aggregates (Fig. 2a, b). (2) Opx-bearing wehrlites have no intact Opx and contain rare corroded Opx surrounded by Cpx. Some of the Opx relics have reaction coronas and patches of newly formed Cpx inside (Fig. 2c). Complex multi-grain Cpx aggregates are common, usually with clear domains set up in fine-grained or inclusion-rich matrix (Fig. 2c). The latter may contain irregularly shaped spinel (e.g. skeletal or resorbed), second-generation olivine, feldspar and vugs. (3) Wehrlites 9510-3 (Fig. 2d) and 9503-22 contain no Opx. They are made up of coarse-grained olivine matrix with grains or clusters of mainly clear, inclusion-free Cpx with smooth curvilinear boundaries (Fig. 2d; fine-grained Cpx rims are of late-stage origin). The Opx-free wehrlites contain only trace amounts of spinel (inclusions in olivine) compared with 0.5–2.5% Spl in low-Opx lherzolites (Table 1).

Our petrographic observations indicate that abundances and appearance of olivine are little affected by the Cpx formation. The metasomatic Cpx-rich aggregates most commonly replace Opx (but not olivine) and develop in the interstitial space at triple junctions of olivine grains (Fig. 2b). In detail, the exact role of olivine in the Opx–Cpx reaction is hard to establish unequivocally from observations in thin sections alone. On one hand, olivine locally has embayed margins in contact with metasomatic Cpx (Fig. 2a), which may indicate minor local consumption of olivine during the Cpx formation. On the other hand, such areas can also be interpreted as new material growing on pre-existing olivine grains. Furthermore, some second-generation olivine occurs inside the newly formed Cpx aggregates and may have been produced as a by-product in the Opx–Cpx reaction. Because olivine and Cpx are texturally equilibrated in Opx-free wehrlites (see earlier text), some re-crystallization during or after the Cpx-forming event is very likely (cf. Fig. 2a, d). Olivine may be locally dissolved and deposited elsewhere in the rock; the net effect of such redistribution cannot be assessed from petrographic observations at millimetre scale. Importantly, the two Opx-free wehrlites, in this study, have higher modal olivine (82–84%; Table 1) than any LH series rock (≤ 80% Ol). Assuming that the LW series is

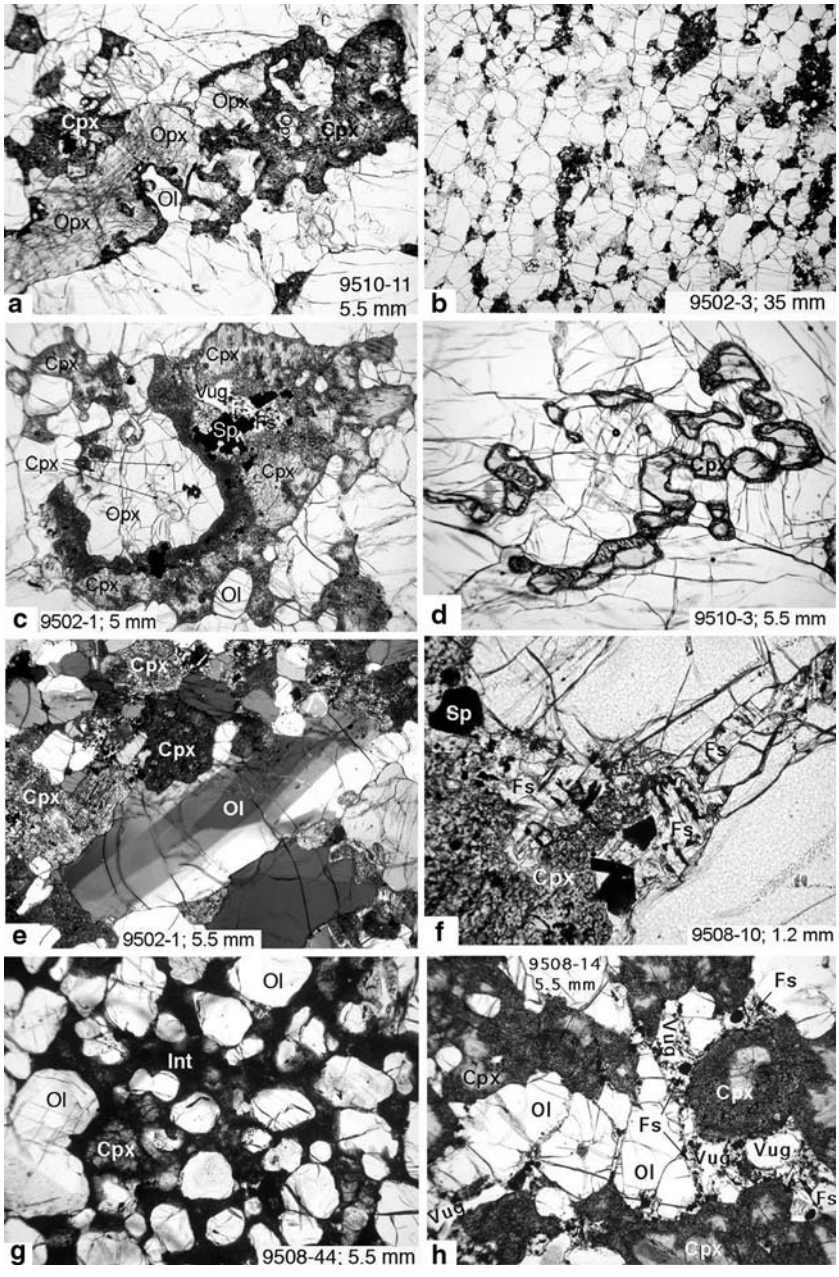

Fig. 2 Photomicrographs of lherzolite–wehrlite series and cumulate Tok xenoliths in plane-polarised (unless noted otherwise) transmitted light. Sample numbers and the field of view are indicated on each plate. *Ol*, olivine; *Opx*, orthopyroxene; *Cpx*, clinopyroxene; *Sp*, spinel; *Fs*, feldspar. **a** Different stages of replacement of Opx by Cpx in lherzolite: from discontinuous thin Cpx rims at Opx grain margins (*down left*) to rare resorbed Opx relics inside newly formed Cpx (*upper right*). Note embayed Ol at the margins and inside the metasomatic Cpx-rich aggregates. **b** Preferred linear orientation of coarse elongated olivine in Opx-poor lherzolite. Newly formed Cpx-rich aggregates (*dark grey*, *cloudy*) mainly replace Opx (*light grey*) and fill interstitial space between the olivine grains. Thus, the Cpx precipitation typically takes place at the expense of Opx and is not accompanied by significant changes in modal Ol. **c** Replacement of Opx by Cpx (with a reaction corona) in wehrlite; *arrows* indicate some newly formed Cpx inside Opx. The Cpx grains have cloudy or spongy domains and locally enclose small vugs, secondary Ol, Sp and alkali Fs. **d** Clusters of clear emerald-green metasomatic Cpx in wehrlite. No Opx and Sp are observed; they have been probably replaced by the Cpx. **e** Crossed analysers. Strained primary Ol and unmixed, twinned secondary Cpx in wehrlite (same sample as in **c**). **f** Interstitial feldspar, Sp and Ti-rich oxides (*small*, *black*) in wehrlite. **g** Ol-rich Ol–Cpx cumulate with quenched cryptocrystalline interstitial material (*Int*). **h** Ol–Cpx cumulate. Spongy rims of Cpx may have formed by reaction of initial cumulate grains with pore liquid (see **g**). Fine-grained interstitial material contains Fs, Sp, Ti-oxides and hosts abundant vugs

formed after the LH series rocks, it is more likely that the small amounts of olivine are produced rather than consumed during the replacement of Opx by Cpx.

Many LW series rocks have linear fabrics due to parallel orientation of elongated olivine grains, which is apparent in spite of widespread Cpx development

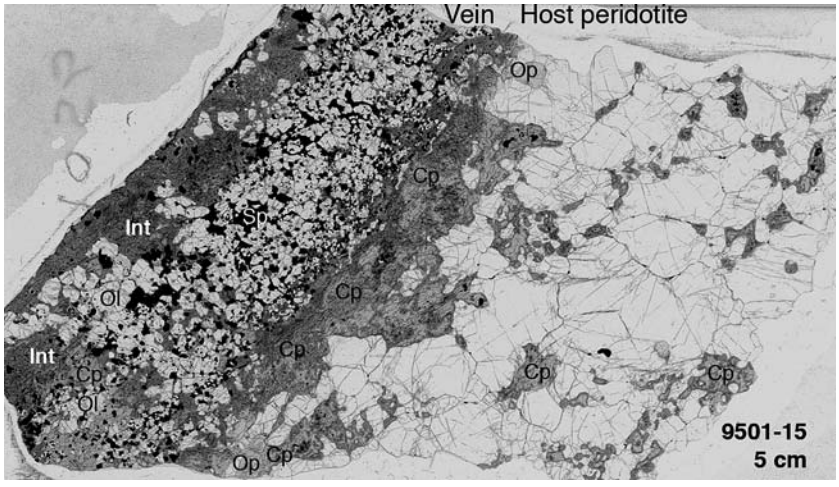

Fig. 3 Photomicrograph of a magmatic vein in an LW series Tok xenolith (plane-polarised transmitted light). The vein ~1.2 cm across is filled with a quenched Ol–Sp–Cpx cumulate. Ol is the main cumulate mineral; euhedral Sp grains are smaller, they are located between Ol; cumulate Cpx is rare (*left bottom*). The fine-grained interstitial material (*Int*) is rare between the cumulate minerals and is concentrated on one side of the vein indicating that the initial magma (or crystal-liquid mush) experienced some in situ gravity segregation after the intrusion such that the dense Ol and Sp crystals precipitated to the bottom of the vein (on the right) leaving behind the lighter residual liquid. Note continuous aggregates of coarse Cpx in the wall-rock peridotite at vein contact, which we consider as metasomatic aureole produced by fluids escaped from the vein

(Fig. 2b). Such textures are also common in olivine-rich LH series rocks. Olivine grains in many wehrlites also exhibit (at crossed polarisers) signs of deformation, such as kink banding, while Cpx cores have abundant Opx exsolution and twinning (Fig. 2e). There are no olivine neoblasts at the contact of coarse strained olivine with the metasomatic Cpx. The evidence for strain and deformation in the olivine grains, together with the absence of cumulate textures rule out cumulate origins for the LW series.

Cumulate xenoliths from Tok were identified in the field by black colour of the Cpx and dark yellow colour of olivine as well as common empty vugs. They have a broad range of olivine and Cpx abundances, grain size and textures. The inter-cumulus ranges from dark cryptocrystalline material (Fig. 2 g) to fine-grained aggregates of late-stage Cpx, feldspar and oxide minerals (Fig. 2 h). In the latter case, the cumulate Cpx has clear cores and fine-grained rims, apparently recrystallised due to the reaction of the original cumulate crystals with trapped interstitial liquid. Importantly, olivine grains in the Ol–Cpx cumulate xenoliths have no kink banding or other signs of deformation (Fig. 2 g, h), unlike olivine in the LW series rocks (Fig. 2e).

Some Tok xenoliths are composite, i.e. contain veins of apparently magmatic origin in LH or LW series peridotites. Figure 3 shows a vein made up of Ol–Spl–Cpx cumulate cross-cutting an Opx-bearing wehrlite. Importantly, coarse metasomatic Cpx is very abundant in the peridotite at the contact with the vein whereas farther from the vein Cpx is much less common and has smaller grain size. Such relationships may indicate links between magmatic events (migration and fractionation of silicate melts) and the formation of metasomatic Cpx in the lithospheric mantle beneath Tok and hence be relevant to the origin of LW series rocks.

The LW series rocks commonly contain accessory metasomatic minerals: amphibole, phlogopite, phosphates, alkali feldspar and Fe–Ti oxides (Table 1). These minerals are not spatially related to the Opx–Cpx replacement zones, they are typically interstitial and their abundances do not exceed 3%. Feldspar forms veins and small pockets together with Fe–Ti oxides and fine-grained or spongy Cpx (Fig. 2f). The feldspar occurs only in the late-stage, fine-grained interstitial materials and is not texturally equilibrated with coarse pyroxenes and spinel. Amphibole and phlogopite have small grain size (0.1–1 mm) and in many cases are completely or partially replaced by fine-grained feldspar, oxides and second-generation Ol, Spl and Cpx as discussed by Ionov et al. (2005b) for the LH series. Similar feldspar-bearing aggregates occur in xenoliths from other sites in southern Siberia (Baikal, Sikhote-Alin); they have been attributed to a specific "anhydrous" type of mantle metasomatism, which takes place shortly before the xenoliths are entrained in the host magma (Ionov et al. 1999).

Like in the LH series, olivine and pyroxenes in many LW series rocks contain abundant fluid inclusions (Table 1); some xenoliths contain irregularly shaped empty cavities (vugs). None of these metasomatic features are spatially or texturally related to host basalt. We assume therefore that the late-stage, secondary minerals, fluid inclusions and vugs formed in the mantle, possibly shortly before the transport of the xenoliths to the surface. Some LW series rocks contain more alkali feldspar (1–2.5%; Table 1) than typical LH series peridotites. In general, however, the assemblages, abundances and

textural position of the accessory minerals in the LW series rocks do not differ significantly from those in the LH series rocks.

Modal abundances in the LW and LH series rocks are shown in Fig. 4. Characteristic of the LW series is a combination of relatively high modal Cpx (≥12%), low Opx (≤ 10%) and high Cpx/Opx (> > 1, typically > 2). Taken together, these parameters clearly distinguish the LW series rocks from those LH series xenoliths (e.g. 9505-3, 9510-16; Fig. 4), in which metasomatic Cpx may have formed as well but on a smaller scale. Modal composition of sample 9510-11 is intermediate between those typical of the two series (Fig. 4a, b). Nevertheless, it obviously belongs to the LW series because of very low Mg# (0.84; Fig. 4c, d) as well as common replacement of Opx by Cpx (Fig. 2a) and higher Cpx/Opx than in the LH series (0.6 compared with 0.2–0.4) at similar modal olivine. Cpx abundances in the LW series rocks do not exceed 23% (Fig. 4a), and the total pyroxene contents (Opx + Cpx; 16–28%) do not appear to be significantly above total pyroxene contents typical of olivine-rich LH series peridotites (Fig. 4c). The modal data further indicate (in addition to textural evidence; Fig. 2a–c) that the high Cpx abundances in the LW series rocks are mainly a result of replacement of Opx (roughly preserving total pyroxene mass) in initially Cpx-poor peridotites while olivine abundances do not change much.

Whole-rock major element compositions

Whole-rock XRF analyses are given in Table 2. The LW series, defined earlier mainly based on textural and modal data (Figs. 2 and 4), can also be clearly identified on major element co-variation diagrams. The LW series rocks form a distinct field on an MgO vs. SiO_2 plot (Fig. 5a) due to a combination of lower MgO and SiO_2 than in the LH series (and other residual mantle peridotites). This is consistent with replacement of Opx (54–57% SiO_2, 32–35% MgO) by Cpx (51–54% SiO_2, 15–17% MgO), which reduces both silica and MgO contents. Furthermore, the contents of FeO in the LW series peridotites are commonly very high (9.4–14.4%; Fig. 5b). Hence, the Fe–Mg substitution in minerals is another reason for generally lower MgO in the LW series than in refractory LH series rocks at similar olivine abundances (Fig. 4). Several LW series rocks define linear Mg–Fe trends in Fig. 5b.

CaO (hosted mainly by metasomatic Cpx) and FeO appear to be distinctive major oxides of the LW series. A CaO vs. FeO diagram (Fig. 6a) clearly distinguishes

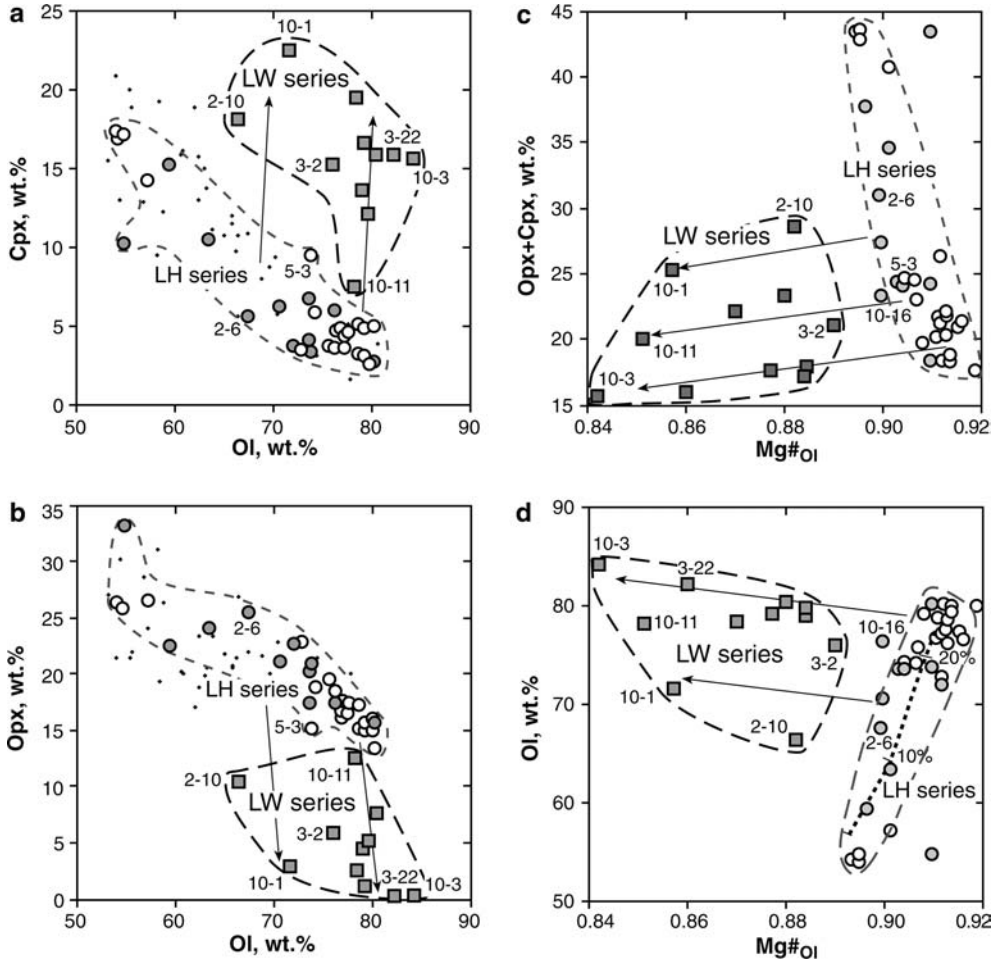

Fig. 4 **a–c** Co-variation plots of modal abundances and $Mg\#_{Ol}$ [$Mg/(Mg+Fe)_{at}$ in olivine] in Tok peridotites. *Filled squares*, lherzolite–wehrlite (LW) series; *circles*, lherzolite–harzburgite (LH) series; *filled circles*, LH xenoliths with heterogeneous Fe–Mn–Ni in Ol (likely enriched in Fe, Mn) (Ionov et al. 2005b). Abbreviated sample numbers are shown for xenoliths discussed in text. *Arrows* outline inferred trends for transformation of refractory LH series rocks into LW series rocks. Shown for comparison are spinel peridotite xenoliths from southern Siberia and Mongolia (Ionov et al. 2005a; Press et al. 1986; Wiechert et al. 1997) (*small black crosses*). *Thick dashed line* in **d** shows batch partial melt extraction residues (0–25%) from fertile peridotite at 2 GPa (Walter 2003)

Table 2 XRF analyses of whole-rock samples

Sa. N°	SiO_2	TiO_2	Al_2O_3	Cr_2O_3	Fe_2O_3	FeO	MnO	NiO	MgO	CaO	Na_2O	K_2O	P_2O_5	LOI	Total	Mg#	Ca/Al	∑FeO
Lherzolite–wehrlite series																		
9502-1	42.16	0.18	1.59	0.31	1.78	9.02	0.22	0.28	39.30	4.03	0.42	0.06	0.05	0.56	100.0	0.868	3.4	10.62
9502-2	42.70	0.17	1.59	0.38	1.32	8.53	0.19	0.28	40.91	2.82	0.35	0.06	0.03	0.61	99.9	0.882	2.4	9.72
9502-3	42.66	0.20	1.55	0.36	1.19	8.88	0.18	0.31	41.05	2.44	0.34	0.10	0.05	0.69	100.0	0.880	2.1	9.95
9502-4	42.25	0.17	1.65	0.34	0.96	9.59	0.19	0.29	39.98	3.20	0.38	0.09	0.06	0.73	99.9	0.872	2.6	10.45
9502-10	43.66	0.27	3.36	0.35	1.54	8.04	0.17	0.27	37.70	3.59	0.50	0.15	0.04	0.75	100.4	0.877	1.4	9.43
9503-2	42.27	0.18	1.38	0.36	0.77	8.66	0.18	0.30	41.87	2.89	0.43	0.09	0.05	0.66	100.1	0.889	2.8	9.35
9503-22	41.49	0.11	0.98	0.35	1.88	10.13	0.21	0.33	40.52	2.96	0.48	0.08	0.06	0.39	100.0	0.859	4.1	11.82
9507-6[b]	42.08	0.10	0.80	0.42	ND	9.91	0.26	0.30	43.78	2.44	0.21	0.05	0.05	n.d.	100.4	0.887	4.1	9.91
9508-10[a]	42.69	0.23	2.03	0.33	ND	9.94	0.15	0.26	40.68	3.38	0.29	0.08	0.06	n.d.	100.1	0.879	2.3	9.94
9510-1[a]	42.36	0.34	2.82	0.32	ND	11.78	0.16	0.20	36.86	4.57	0.35	0.08	0.05	n.d.	99.9	0.848	2.2	11.78
9510-3	41.34	0.09	0.76	0.36	0.46	13.12	0.24	0.30	39.47	2.82	0.43	0.03	0.04	0.68	100.1	0.839	5.0	13.53
9510-11[a]	42.13	0.05	0.82	0.35	ND	14.38	0.21	0.25	39.09	1.57	0.20	0.07	0.23	n.d.	99.3	0.829	2.6	14.38
Olivine-cpx cumulate and host basalt																		
9508-14	45.76	1.18	6.55	0.38	2.12	6.57	0.14	0.09	20.24	15.39	0.90	0.14	0.06	0.67	100.2	0.810	3.2	8.48
9508-1b	45.22	2.37	14.69	0.03	2.48	7.51	0.17	0.05	9.38	8.46	4.57	3.37	1.09	0.34	99.7	0.632	0.8	9.74

ND, not determined; Mg#, $Mg/(Mg + Fe)_{at}$. Fe_2O_3 and loss on ignition (LOI) were only determined at FMC; total Fe is shown as FeO for analyses done at Niigata and Mainz

[a]Analyzed at Niigata University

[b]Analysed at Mainz University

the LW and LH series. The majority of LW series rocks define a trend of marked enrichments both in CaO (2.4–4.6%) and FeO (9.5–12%), whereas xenolith 9510-11 has high FeO (14.4%) at moderate Ca (Fig. 6a) consistent with fairly low modal Cpx in that sample (Fig. 4a). The contents of Ca at given Al are usually higher in the LW series than in the LH series (Fig. 6b). The range of Al_2O_3 in LW series rocks extends to higher values (up to 3.4%) than in olivine-rich (>66%) LH series rocks (Fig. 6b) possibly indicating moderate Al-enrichments at higher Ca due to high Al in the metasomatic Cpx (see "Mineral compositions and *T* estimates").

Among minor oxides, the contents of MnO and TiO_2 in the LW series show much broader variation ranges and are typically higher than in olivine-rich LH series rocks (Fig. 7); the two series form distinct fields on a Mn–Ti plot (Fig. 7b). MnO in LW series rocks is positively correlated with FeO (Fig. 7a) but negatively correlated with TiO_2 (Fig. 7b). There is some similarity between the Mn–Ti and Fe–Ca (Fig. 6a) plots because strong enrichments in Mn (and Fe; both mainly hosted by olivine) are decoupled in some LW series rocks from enrichments in Ti (and Ca; both mainly hosted by Cpx); hence, distinct enrichment trends can be outlined. The contents of NiO and Cr_2O_3 in the LW series (Fig. 8a) are lower than in refractory LH series rocks (>66% Ol) but they overlap the field of fertile LH series lherzolites. High Na_2O (>0.2%) and K_2O (≥0.05%) in the LW series rocks (Fig. 8b) are consistent with ubiquitous accessory alkali feldspar (Fig. 2f); much Na may also reside in metasomatic Cpx (see "Mineral compositions and *T* estimates"). K/Na in the xenoliths are different from those in the host basalt (Fig. 8b). Overall, our petrographic and chemical data, as well as sample preparation methods, rule out the origin of high K and Na by contamination of the xenoliths with host volcanic material or by post-eruption alteration.

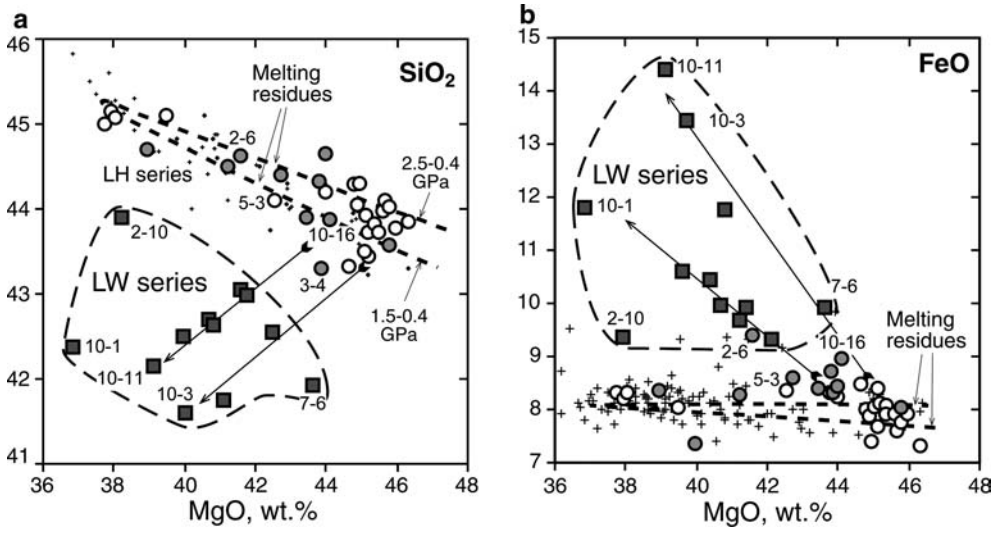

Fig. 5 Plots of MgO vs. SiO_2 (**a**) and FeO (**b**) in whole-rock xenoliths (wt % recalculated to 100% anhydrous, all Fe as FeO). Symbols and data sources are as in Fig. 4. *Thick dashed lines* are calculated residues from polybaric (2.5–0.4 and 1.5–0.4 Ga) fractional melting of fertile lherzolite (Niu 1997; Takazawa et al. 2000)

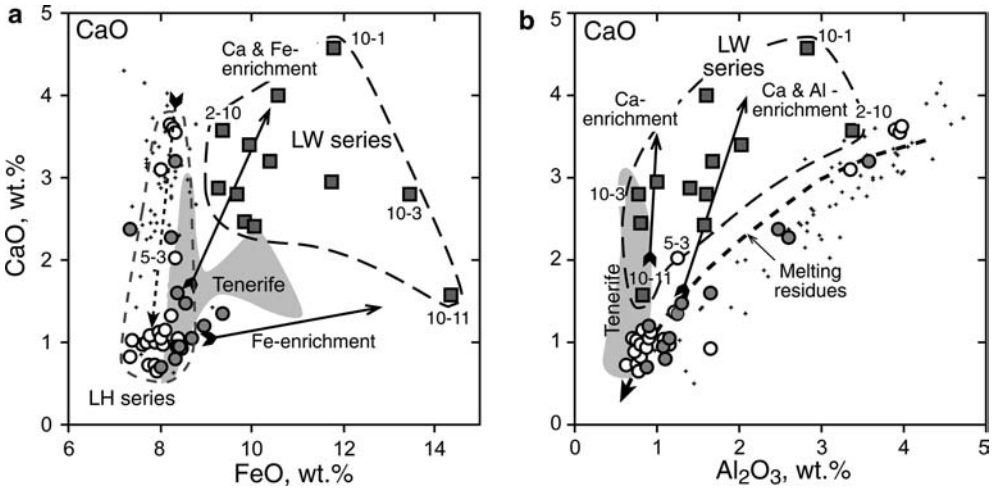

Fig. 6 Plots of CaO vs. FeO (**a**) and Al_2O_3 (**b**) for Tok xenoliths. Symbols and data sources are as in Figs. 4 and 5. Also shown is a field (*grey*) for peridotite xenoliths from Tenerife (Canary Islands) inferred to have been affected by carbonatite metasomatism (Neumann et al. 2002)

Mineral compositions and *T* estimates

Electron probe microbeam analyses for major minerals are given in Table 3 (high-precision data from Mainz are listed for olivine). Table 4 gives analyses of metasomatic minerals and second-generation Ol, Cpx and Spl. Olivine in the LW series rocks has distinctly higher FeO and MnO and lower NiO and Mg#, as well as much broader variation ranges, than in the LH series (Fig. 9). The contents of Mn and Ni and Mg# in olivine in the two series are distinct and hence their fields are clearly apart on the olivine plots (Fig. 9). By contrast, the contents of Mn and Ni in whole-rock LW and LH series peridotites partly overlap (Figs. 7 and 8a). Furthermore, the Mg#–Ni–Mn trends for olivine generally lie along the extensions of combined trends for olivine from the LH series xenoliths, abyssal and cratonic peridotites. Such trends are likely to be controlled by mineral–melt equibria (Boyd et al. 1997; Pearson et al. 2003; Takazawa et al. 2000).

Ionov et al. (2005b) found that olivine in some LH series rocks is not homogeneous because reproducibility of individual EPMA is worse than for the olivine standard measured in the same session. Significant grain-to-grain variations (1σ/mean 1–10% for FeO and 0.1–1.9% for Mg#) have been found for olivine in all the LW series xenoliths (Table 3). Most heterogeneous is olivine 9510-11, with individual EPMA ranging from 12.4 to 16.6% FeO (Mg# 0.872–0.825). Routine EPMA of coarse, strained olivine in xenoliths 9502-1 and 9502-4 (Table 4) did not find significant core–rim differences for Mg# (also if the rims are in contact with metasomatic Cpx; Fig. 2e), but yielded higher Ca and Mn and lower Ni in the rims.

The range of Cr# in spinel [$Cr\#_{Spl} = Cr/(Cr+Al)_{at}$] is identical in the LW and LH series rocks (0.1–0.65); however, $Cr\#_{Spl}$ in the majority of LW series xenoliths is ≤ 0.4 and hence somewhat lower than in olivine-rich LH series xenoliths (Figs. 10 and 11a). $Cr\#_{Spl}$ is negatively correlated with $Mg\#_{Spl}$, but the LW and LH series spinels yield distinct Mg#–Cr# trends because the LW series spinels have lower Mg# at given Cr# (Fig. 10). Spinels in the LW series have higher TiO_2 (0.2–1.1%) than in the LH series ($\leq 0.3\%$). $Cr\#_{Spl}$ does not appear to be correlated with $Mg\#_{Ol}$ in the LW series (Fig. 11a).

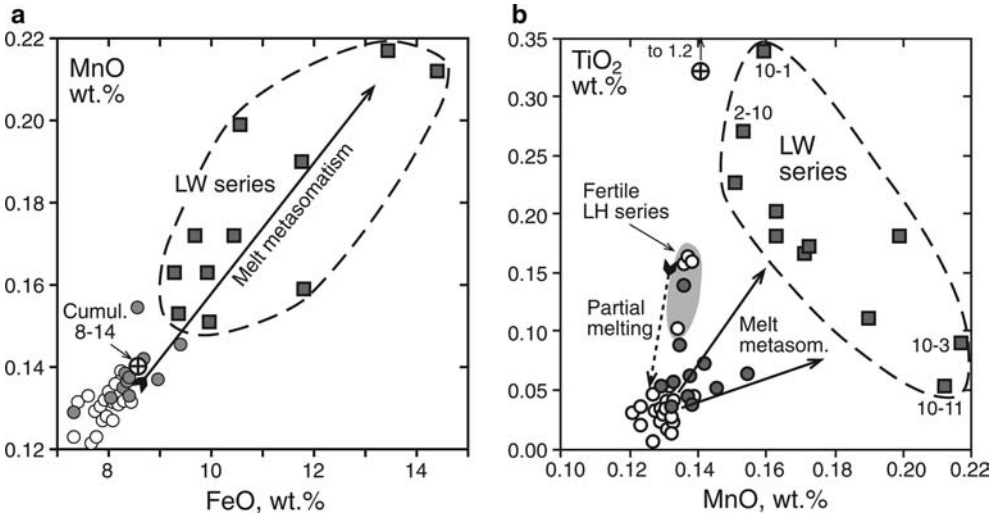

Fig. 7 Plots of MnO vs. FeO (**a**) and TiO_2 (**b**) in Tok xenoliths. *Circled cross* is Ol–Cpx cumulate 9508-14; other symbols are as in Fig. 4. MnO is positively correlated with FeO and negatively correlated with TiO_2 in the LW series. The differences between the Mn–Fe and Mn–Ti trends in the LW series may be related to the fact that Mn and Fe reside mainly in olivine while Ti mainly resides in Cpx and Fe–Ti oxides (Figs. 4, 6a and 7b)

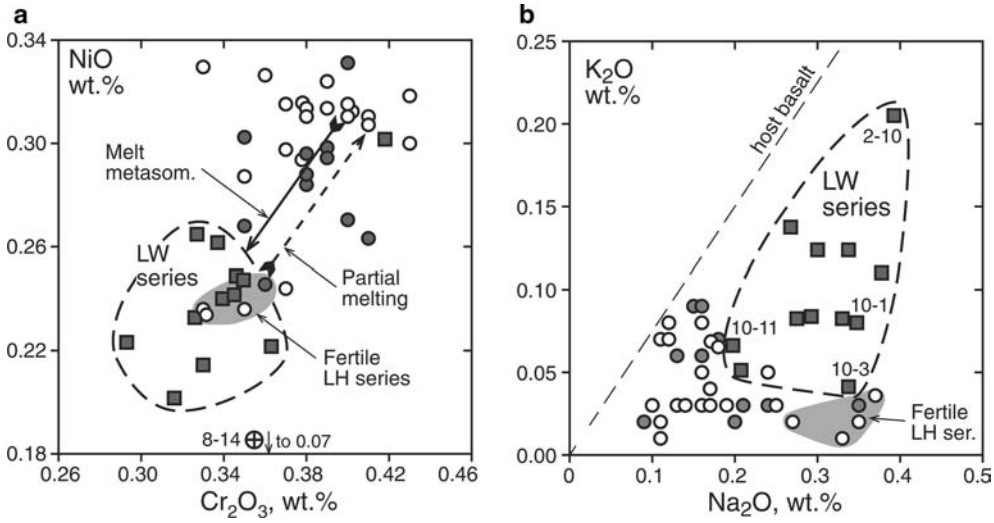

Fig. 8 Plots for Cr_2O_3 vs. NiO (**a**) and Na_2O vs. K_2O (**b**) in Tok xenoliths. Symbols are as in Fig. 4. The LW series rocks have lower Cr and Ni and in many cases also higher Na_2O vs. K_2O than in olivine-rich LH series rocks. *Dashed line* in **b** shows K_2O/Na_2O in host basalt

The combination of relatively low $Mg\#_{Ol}$ (≤ 0.88) with high $Cr\#_{Spl}$ is not unique to the Tok LW series peridotites. Some Fe-enriched, refractory xenoliths from ocean islands (Samoa, Kerguelen, Tenerife) and off-craton continental areas (SW USA) plot close to the Tok LW series in Fig. 11.

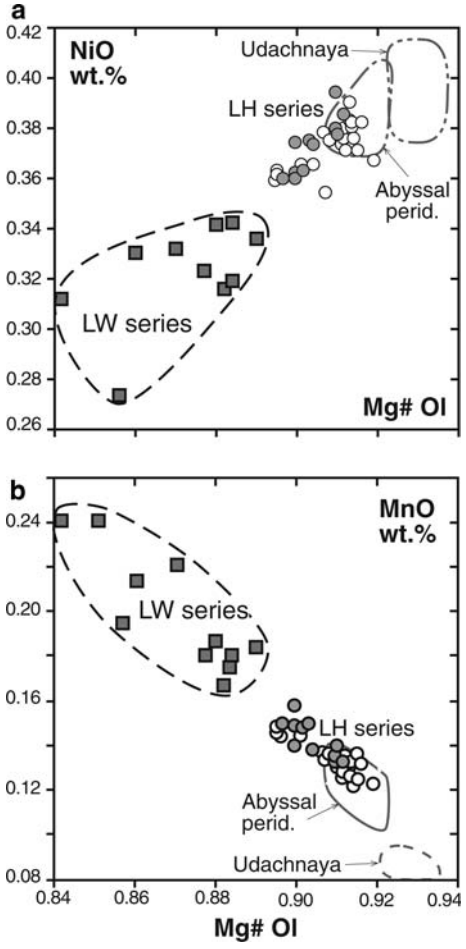

Fig. 9 Plots of Mg# vs. NiO (**a**) and MnO (**b**) in olivine in Tok xenoliths. Symbols are as in Fig. 4. Also shown are fields for spinel peridotite xenoliths from Udachnaya (Boyd et al. 1997) and abyssal peridotites (Hellebrand et al. 2002). Note that the distinction between the LW and LH series fields in **b** is more marked than on the whole-rock Fe–Mn plot (Fig. 7a)

The ranges of Al_2O_3 (3.5–6.7%) and TiO_2 (Fig. 11b) in Cpx from the LW series mainly overlap those for Cpx from the LH series as a whole, but Al and Ti tend to be higher in Cpx from the LW series than in Cpx from olivine-rich LH xenoliths. The two series form distinct fields in Fig. 11b ($Mg\#_{Ol}$–Ti_{Cpx}) because of differences in $Mg\#_{Ol}$ and high Ti in Cpx 9510-1. Cpx in many LW series rocks have high Na_2O and Cr_2O_3, but strong enrichments in Na and in particular in Cr are less common than for LH series Cpx (Fig. 12).

Equilibration temperatures (T) were estimated from the EPMA using the Ca-in-Opx method of Brey and Köhler (1990) (Table 1). They are not given for xenoliths 9502-1 and 9502-4 because their Opx yield variable and usually very high CaO (0.8–1.8%, Table 3) and contain abundant Cpx inclusions (Fig. 2c). The T range for the LW series rocks (908–1024°C) seems to be somewhat higher than for olivine-rich LH xenoliths but those minor differences may be due to local Ca-enrichments related to replacement of Opx by Cpx or incomplete re-equilibration to an ambient geotherm after the Cpx formation event. Hence, the LW series xenoliths appear to come from the same depth range as the LH series (40–60 km, Ionov et al. 2005b).

Second-generation Ol, Cpx and Spl in the LW series (as well as in the LH series) differ in composition from the primary minerals (Table 4). Second-generation olivine usually has higher Ca and Mn and lower Ni than coarse olivine. Fine-grained and spongy Cpx co-existing with feldspar typically have lower Na and Al and higher Ti than primary Cpx as well as significant Al and Cr grain-to-grain variations (Table 4). The compositions of phlogopite, amphibole and feldspar are similar to those in the LH series xenoliths. In particular, the feldspar is commonly alkali-rich, a feature consistent with high K and Na in the bulk rocks (Fig. 8b).

Table 3 EPMA for major minerals (average of representative analyses)

Sa.N°	9502-1	9502-2	9502-3	9502-4	9502-10	9503-2	9503-22	9508-10	9510-1	9510-3	9510-11	9508-14
Olivine (averages of eight grain cores each)												
SiO_2	40.50	40.83	40.73	40.67	40.90	41.04	40.66	40.56	40.32	40.02	40.04	39.10
Al_2O_3	0.010	0.007	0.009	0.005	0.023	0.009	0.010	0.009	0.013	0.012	0.012	0.01
Cr_2O_3	0.007	0.012	0.009	0.008	0.008	0.012	0.014	0.005	0.006	0.016	0.025	0.00
FeO	12.56	11.37	11.35	11.71	11.57	10.81	13.58	11.89	13.83	15.13	14.34	18.38
1σ/mean (%)	2	1	2	2	1	2	4	4	4	3	10	4
MnO	0.22	0.18	0.18	0.19	0.17	0.18	0.21	0.18	0.20	0.24	0.24	0.22
NiO	0.33	0.32	0.34	0.34	0.32	0.34	0.33	0.32	0.27	0.31	0.33	0.13
MgO	47.30	48.43	48.29	48.09	48.48	49.03	46.89	47.55	46.43	45.11	45.88	42.66
CaO	0.045	0.039	0.040	0.037	0.066	0.046	0.057	0.048	0.049	0.052	0.052	0.036
Total	101.0	101.2	100.9	101.1	101.5	101.5	101.8	100.5	101.1	100.9	100.9	100.6
Mg#	0.870	0.884	0.884	0.880	0.882	0.890	0.860	0.877	0.857	0.842	0.851	0.805
1σ/mean (%)	0.3	0.2	0.3	0.3	0.1	0.3	0.6	0.6	0.8	0.6	1.9	1.1
Spinel												
SiO_2	0.08	0.04	0.04	0.05	0.07	0.06	0.05	0.09	0.11	0.12	0.09	
TiO_2	0.95	0.48	0.46	0.37	0.20	0.50	1.09	0.34	0.42	1.01	0.25	
Al_2O_3	31.60	32.53	39.77	39.85	57.08	32.86	22.31	43.95	52.96	17.34	28.52	
Cr_2O_3	33.13	35.37	28.01	27.04	9.01	32.94	38.95	23.18	12.46	44.10	37.45	
FeO	19.51	15.66	13.82	15.70	12.66	16.62	24.02	13.91	14.48	24.68	18.63	
MnO	0.00	0.22	0.23	0.22	0.17	0.22	0.31	0.22	0.14	0.34	0.26	
MgO	14.42	15.13	17.03	16.14	20.13	15.48	11.51	17.38	18.15	9.84	13.04	
NiO	0.21	0.10	0.17	0.19	0.25	0.12	0.16	0.16	0.21	0.10	0.14	
Total	99.9	99.5	99.5	99.6	99.6	98.8	98.4	99.2	98.9	97.5	98.4	
Mg#	0.57	0.63	0.69	0.65	0.74	0.62	0.46	0.69	0.69	0.42	0.55	
Cr#	0.41	0.42	0.32	0.31	0.10	0.40	0.54	0.26	0.14	0.63	0.47	
Orthopyroxene												
SiO_2	53.45	55.95	56.02	53.13	54.67	56.55		55.57	54.84	55.24	55.51	
TiO_2	0.22	0.00	0.01	0.28	0.07	0.01		0.06	0.09	0.07	0.02	
Al_2O_3	3.87	1.81	1.74	4.70	4.28	1.32		2.95	3.30	1.73	2.18	
Cr_2O_3	0.75	0.34	0.34	0.74	0.38	0.38		0.37	0.27	0.45	0.46	
FeO	7.86	6.80	7.11	7.88	7.47	6.69		6.89	9.07	9.24	8.81	
MnO	0.22	0.19	0.15	0.22	0.17	0.19		0.19	0.19	0.29	0.22	
MgO	31.45	34.22	33.93	31.33	32.32	34.02		33.11	31.42	31.20	31.87	
CaO	1.62	0.53	0.53	1.57	0.88	0.64		0.75	0.68	0.73	0.55	
Na_2O	0.15	0.07	0.08	0.18	0.20	0.10		0.12	0.08	0.20	0.17	
NiO	0.10	0.06	0.08	0.09	0.05	0.05		0.06	0.05	0.07	0.04	
Total	99.7	100.0	100.0	100.1	100.5	100.0		100.1	100.0	99.2	99.8	
Mg#	0.877	0.900	0.895	0.876	0.885	0.901		0.895	0.861	0.857	0.866	
Clinopyroxene												
SiO_2	51.12	51.86	52.41	52.90	52.64	53.29	52.98	52.03	50.48	52.78	52.18	49.35
TiO_2	0.58	0.41	0.09	0.13	0.12	0.11	0.18	0.49	1.01	0.34	0.31	1.18
Al_2O_3	5.86	4.95	4.62	4.38	5.12	3.51	3.95	5.44	6.74	4.42	3.49	7.58
Cr_2O_3	1.54	1.70	2.11	1.59	0.90	1.34	1.68	1.38	1.05	1.94	2.28	0.78
FeO	3.58	2.91	2.96	3.24	3.79	3.50	3.78	2.97	3.59	4.36	4.52	5.03
MnO	0.11	0.13	0.12	0.09	0.13	0.12	0.10	0.11	0.12	0.16	0.16	0.11
MgO	14.85	15.32	15.41	15.98	16.40	17.03	15.65	15.27	14.58	14.45	16.60	14.42
CaO	20.11	20.09	19.37	19.26	18.26	17.80	18.07	19.39	19.88	17.05	17.71	20.27
Na_2O	1.71	1.79	2.20	1.95	1.97	2.08	2.35	1.82	1.50	2.87	1.33	1.08
NiO	0.04	0.02	0.05	0.03	0.04	0.01	0.02	0.03	0.02	0.04	0.06	0.03
Total	99.5	99.2	99.3	99.6	99.4	98.8	98.8	98.9	99.0	98.4	98.6	99.8
Mg#	0.881	0.904	0.903	0.898	0.885	0.897	0.881	0.902	0.879	0.855	0.868	0.836
Cr#	0.15	0.19	0.23	0.20	0.11	0.20	0.22	0.15	0.09	0.23	0.30	0.06

Trace element compositions of whole-rock xenoliths

Trace element compositions of two wehrlites, one cumulate and host basalt are given in Table 5; their patterns are shown in Fig. 13. The abundances of heavy and middle REE in the LW series rocks are much higher than in olivine-rich LH series rocks (Ionov et al. 2005b; D.A. Ionov et al. submitted for publication). Furthermore, the wehrlites typically have concave-upward REE and extended trace element patterns, which are similar to those of cumulate 9508-14, but distinct from the commonly LREE-enriched patterns of olivine-rich LH series rocks (Fig. 13). Because cumulate 9508-14 is likely to be equilibrated with its parental magma, the similarity of its pattern with those of the LW rocks may indicate that the latter were completely or partially equilibrated with liquids with similar trace element patterns. By contrast, the LW series rocks have negative Pb and Ti anomalies, which are absent or much less-developed in the cumulate and the host basalt. Big differences in the relative and absolute abundances of highly incompatible

Table 4 EPMA for metasomatic and second-generation minerals

	9502-3	9502-4	9503-2	9502-1	9502-4	9503-22	9502-1				9502-4				
	Am	Am	Phl	Fs	Fs	Fs	Ol, core	Ol, rim	Ol-2nd	Spl-2nd	Ol core	Ol rim	Ol-2nd	Cpx	Cpx-2nd
SiO_2	41.53	41.03	37.29	56.79	64.09	54.27	39.44	38.64	38.82	0.10	40.12	40.08	39.06	49.90	51.32
TiO_2	5.37	5.16	4.80	0.25	0.45	1.47				0.32				0.88	1.07
Al_2O_3	13.71	13.57	15.90	26.10	20.16	23.60				41.74				7.14	4.03
Cr_2O_3	1.61	1.17	1.24	0.02		0.06				24.17				1.19	0.58
FeO	4.23	5.36	4.66	0.26	0.18	1.61	13.14	12.69	13.26	17.94	13.29	13.32	12.34	3.82	3.55
MnO	0.08	0.07	0.02				0.25	0.29	0.37		0.23	0.25	0.27	0.10	0.10
MgO	15.57	15.73	20.49	0.04		0.16	47.22	47.12	46.60	15.98	47.42	47.06	47.88	14.73	16.82
CaO	10.86	10.48	0.03	7.78	1.06	0.48	0.05	0.15	0.23		0.04	0.16	0.20	19.07	22.22
Na_2O	2.70	2.76	1.08	6.21	5.45	5.85								1.84	0.39
K_2O	1.57	1.81	9.34	0.78	7.63	8.79									
NiO	0.07	0.10	0.17				0.33	0.30	0.26	0.23	0.35	0.34	0.27	0.03	0.03
Total	97.3	97.2	95.0	98.2	99.0	96.3	100.5	99.3	99.7	100.5	101.5	101.2	100.0	98.7	100.2
Mg#	0.87	0.84	0.89				0.86	0.87	0.86	0.61	0.86	0.86	0.87	0.87	0.894

Blank entries: below detection limit. 2nd (second-generation), fine-grained minerals inside vugs and at grain boundaries.*Ol*, olivine; *Cpx*, clinopyroxene; *Spl*, spinel; *Phl*, phlogopite; *Am*, amphibole; *Fs*, feldspar

elements between the LW series rocks and the host basalt rule out significant entrapment of host magma during or shortly before the eruption. In particular, they further indicate that the late-stage interstitial material in the peridotites formed by mantle metasomatism.

Discussion

Nature of protoliths for the LW series rocks

We first summarize petrographic and chemical evidence against cumulate origins for the LW series. The LW peridotites have no cumulate textures; many show strain and deformation in coarse olivine grains (Fig. 2e), whereas olivine in cumulates is not strained. Many LW series xenoliths contain Opx, whereas no primary Opx has been found in cumulate Tok xenoliths. Whole-rock cumulate 9508-14 contains more Ti, Al, Ca, Na, REE and HFSE (Fig. 13), and less Mg and Ni than the LW series rocks (e.g. it is out of scale in Figs. 5, 6, 7, 8). Olivine 9508-14 has lower Mg# (0.805) and NiO (0.13%) than olivine in LW series rocks (Mg#, 0.84–0.89; NiO, 0.27–0.34%). Cpx 9508-14 has higher Ti and Al and lower Na, Cr# and Mg# than any LW series Cpx (Table 3). In addition, a Re–Os and PGE study of Tok xenoliths (Ionov et al. 2001; D.A. Ionov et al. submitted for publication) found high abundances of Os in LW series xenoliths 9508-10 and 9510-3 (2.3–3.0 ppb), which fall in the range of LH series rocks (0.9–3.9 ppb) but are two orders of magnitude higher than in cumulate 9508-14 (0.02 ppb) or crystallization products of mantle-derived magmas in general (Shirey and Walker 1998).

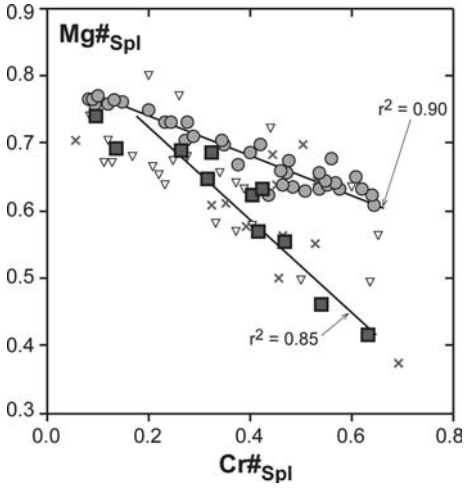

Fig. 10 A plot of Cr# [$Cr/(Cr+Al)_{at}$] vs. Mg# in spinel. Symbols and data sources are as in Fig. 4. Linear regression lines and correlation coefficients are given separately for the LH and LW series. Also shown are data for ocean islands (*diagonal crosses*): Samoa (Hauri and Hart 1994), Kerguelen (Grégoire et al. 2000), Tenerife (Neumann et al. 2002), and Fe-rich continental off-craton xenoliths (*upside-down triangles*) (Ionov et al. 2005b; Smith 2000)

Because a cumulate origin for the LW series can be definitively ruled out, the only plausible alternative is a derivation from residual mantle peridotites, like LH series rocks. Indeed, several lines of petrographic evidence directly link the LW series to refractory LH series peridotites as most likely protoliths. The key argument is the replacement of Opx by Cpx, in particular that consecutive stages of that process can be identified in thin sections (Fig. 2a–d) and matched to the decrease in calculated modal Opx in individual xenoliths (Table 1) from abundances only slightly lower than in the LH series to zero (Fig. 4b). Furthermore, olivine abundances in the LW series and refractory LH series rocks are similar (mainly 70–80%; Fig. 4a, b), consistent with petrographic data that show (a) no significant replacement of olivine in the LW series rocks and (b) that total pyroxene abundances (Opx + Cpx) in the LW series rocks are not higher than in refractory LH series rocks (Fig. 4c).

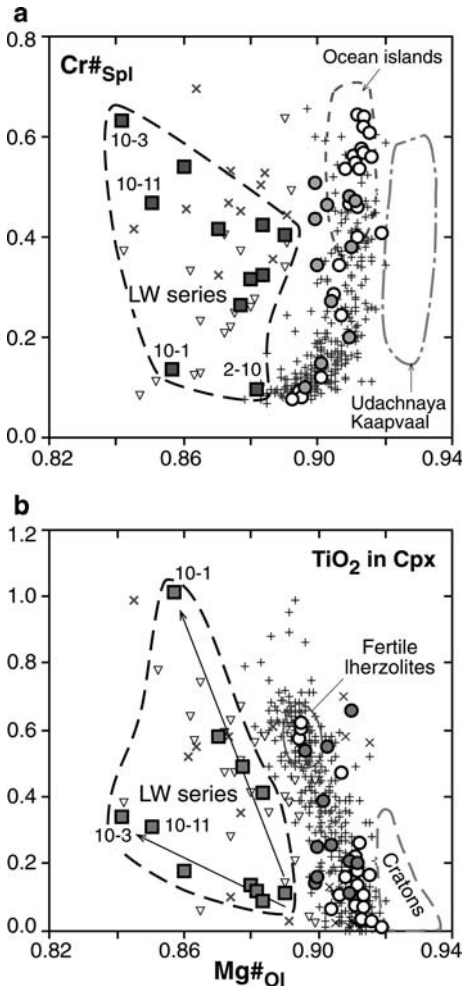

Fig. 11 Co-variation diagrams for $Mg\#_{Ol}$ vs. $Cr\#_{Spl}$ (**a**) and TiO_2 (wt %) in Cpx (**b**). Symbols and data sources are as in Figs. 4, 9 and 10. See Ionov et al. (2005b) for additional data sources on continental spinel peridotite xenoliths (*crosses*)

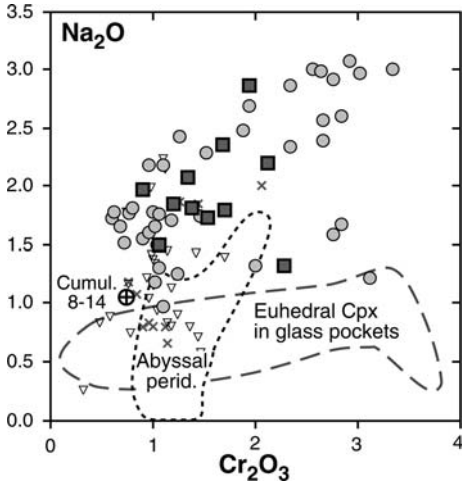

Fig. 12 A plot of Na_2O vs. Cr_2O_3 (wt %) in Cpx from Tok xenoliths (symbols and data sources are as in Figs. 9 and 10). *Dashed line* outlines a field of Cpx micro-phenocrysts in silicate glass pockets in mantle xenoliths [data sources in Ionov et al. (2005b)]

Finally, the observation that practically intact Opx grains can co-exist in LW series lherzolites with strongly resorbed Opx (Fig. 2a, b) indicates an open-system reaction with heterogeneously distributed percolating fluid and argues against simultaneous Opx breakdown, which could be attributed to a closed-system change in *P–T* conditions. Small, fine-grained Cpx-rich metasomatic aggregates commonly occur at triple junctions of olivine grains (Fig. 2b) and hence may be related to melt percolation because olivine triple junctions are more permeable for silicate liquids than Ol–pyroxene or pyroxene–pyroxene grain boundaries because of mineral–melt wetting properties (Faul 1997; Toramaru and Fujii 1986).

Modal and chemical trends in the LW series

The previous section has established, mainly using petrographic evidence, that the LW series was likely formed by transformation of refractory melt extraction residues, similar to those of the LH series, caused by percolation of metasomatic melts. The petrographic data lead us to accept as the most likely hypothesis that a key process in the formation of the LW series was replacement of Opx by Cpx (roughly preserving total pyroxene mass) in initially Cpx-poor LH series peridotites rather than dissolution of olivine accompanied by crystallization of Cpx. The chemical data indicate that another key process in the formation of the LW series was enrichment in iron and related chemical changes in bulk rocks and minerals. In the following text, we use the combined chemical and petrographic evidence to further explore these processes, constrain their mechanisms and outline compositions of the metasomatic media.

We envisage that peridotite protoliths for the LW series contained some 65–80% Ol, 13–23% Opx and 2–10% Cpx (Fig. 4a–c). Modal and chemical trends inferred for the generation of LW series rocks are shown by arrows in Figs. 4, 6, 7, 8 and 11. The arrows are parallel to each other on modal plots (Fig. 4) because the abundances of olivine and Opx + Cpx probably remained nearly constant. The majority of LW series rocks have high modal olivine (75–84%) because olivine-rich rocks (72–80% Ol) are by far most common among their LH series predecessors and because olivine-rich peridotites are highly permeable for silicate melt percolation (Faul 1997; Toramaru and Fujii 1986; Zhu and Hirth 2003). Protoliths of xenoliths 9502-10 and 9510-1 appear to have contained $\leq 70\%$ Ol. It follows from data in Fig. 4 that marked decreases in $Mg\#_{Ol}$ (≥ 0.90 to 0.84) took place at nearly constant or slightly increasing (up to 4%) olivine abundances.

The magnitudes of inferred changes in modal Cpx and $Mg\#_{Ol}$ match each other well for some xenoliths, for example Cpx-rich (and Opx-free) wehrlites 9503-22 and 9510-3 (Fig. 4a, b) also have very low $Mg\#_{Ol}$ (0.84–0.86; Fig. 4c, d). By contrast, lherzolite 9510-11 has lowest

Table 5 Solution ICPMS analyses of xenoliths and host basalt

Rock Sa.N°	Basalt 9508-1b	Wehrlite 9503-22	Wehrlite 9510-3	Cumulate 9508-14
Li	8.3	2.5	4.1	1.7
Sc	16.2	8.5	8.2	39.4
Ti	13,563	705	632	7,211
V	187	35	33	254
Co	45	103	114	60
Ni	185	1,984	2,149	380
Cu	44	4.3	2.0	39
Rb	32.9	1.07	0.43	1.86
Sr	1,131	61.7	72.6	125
Y	22.2	3.25	3.87	11.0
Zr	252	33.2	33.2	44.4
Nb	80.2	3.82	1.31	2.46
Cs	0.51	0.026	0.002	0.02
Ba	466	19.9	6.47	39.7
La	49.6	1.64	1.59	3.61
Ce	98.3	5.32	5.17	10.9
Pr	10.7	0.86	0.81	1.72
Nd	43.7	4.60	4.34	9.37
Sm	8.21	1.18	1.17	2.71
Eu	2.71	0.40	0.41	0.98
Gd	7.21	1.12	1.19	3.02
Tb	0.94	0.150	0.17	0.44
Dy	5.16	0.83	0.98	2.64
Ho	0.88	0.14	0.17	0.47
Er	2.17	0.33	0.41	1.14
Tm	0.27	0.041	0.051	0.14
Yb	1.62	0.23	0.30	0.80
Lu	0.23	0.034	0.045	0.11
Hf	5.36	0.79	0.72	1.58
Ta	4.21	0.18	0.08	0.18
Pb	3.65	0.10	0.11	0.86
Th	5.38	0.066	0.042	0.20
U	1.77	0.031	0.019	0.091

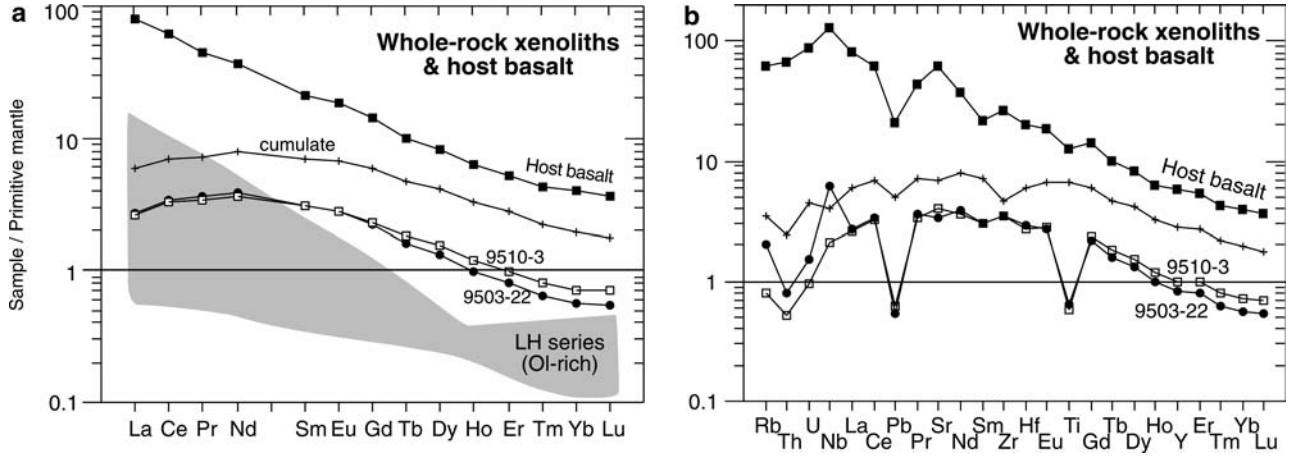

Fig. 13 Primitive mantle-normalised (Hofmann 1988) REE (**a**) and multi-element (**b**) abundance patterns of LW series and cumulate xenoliths and a host basalt. Grey field shows the field of olivine-rich LH series xenoliths (Ionov et al. 2005b). The xenolith patterns are consistent with equilibration of the Cpx in the rocks with a liquid similar to the host basalt but rule out significant contamination of the xenoliths with the host magma

modal Cpx and highest Opx in the LW series, but its $Mg\#_{Ol}$ (0.85) is as low as in the Opx-free wehrlites. Distinct trends or a broad scatter of data points are common on plots of major or minor oxides in whole-rock LW series xenoliths. Two Fe-enrichment trends can be seen on the MgO–FeO diagram (Fig. 5b). The enrichments (relative to refractory LH series rocks) in Ca and Fe (Fig. 6a) or in Mn and Ti (Fig. 7b) are not always proportional to each other. Furthermore, two trends with different slopes of negative $Mg\#_{Ol}$–Ti_{Cpx} correlation can be outlined within the LW series in Fig. 11b.

Different trends of enrichment either in Ca or in Fe are apparent also for some other peridotite suites with abundant metasomatic Cpx, such as olivine-rich xenoliths from the island of Tenerife (Neumann et al. 2002), which appear to have formed after a refractory protolith with a narrow range of Ca, Al and Fe (Fig. 6a). The absence of a uniform Ca-enrichment trend for the LW series on the $CaO–Al_2O_3$ plot (Fig. 6b) may indicate that enrichments in Ca (due to Cpx formation) may have been accompanied by variable enrichments in Al, consistent with particularly high Al_2O_3 (5.1–6.7%; Table 3) in Cpx from those LW series xenoliths that have high whole-rock Al_2O_3 (>2%; Fig. 6b). By comparison, the metasomatic peridotites from Tenerife are not enriched in Al (Fig. 6b) and contain Al-poor Cpx.

The nature of the metasomatic liquids

Some of the chemical and modal variations in the LW series outlined in the previous section can be attributed to the range of modal (Fig. 4) and chemical (Figs. 5, 6) compositions in its parental rocks. In most cases, however, they can be better explained by chemical variations in the metasomatic melts, in particular in Mg#. Relatively high $Cr\#_{Spl}$ and the absence of trends on the $Mg\#_{Ol}$–$Cr\#_{Spl}$ diagram (Fig. 11a) indicate that $Cr\#_{Spl}$ in the LW series xenoliths was less affected by the metasomatism than Mg# in minerals, possibly because of low solubility of Cr in basaltic melts equilibrated with Cr-Spl (Liu and O'Neill 2004).

An essential feature of the metasomatic media responsible for the formation of the LW series is a capacity to react with Opx to produce Cpx. On one hand, this indicates that the melt was undersaturated in silica and thus out of equilibrium with the silica-rich Opx. Furthermore, it was relatively rich in Ca because otherwise it could have dissolved Cpx as well to produce harzburgites and dunites as documented in some mantle peridotite series worldwide (Batanova et al. 1998; Bodinier and Godard 2003; Kelemen et al. 1992; Tommasi et al. 2004; Xu et al. 2003).

Some authors attributed the origin of mantle wehrlites to carbonatite or carbonate-rich silicate melts (e.g. Hauri et al. 1993; Neumann et al. 2002; Yaxley et al. 1991). Several lines of evidence indicate that such an origin is unlikely for the Tok LW series. Mantle carbonate-rich melts typically have high Mg# and are not likely to produce a range of relatively low Mg# in a peridotite series (e.g. Dalton and Wood 1993). Unreasonably large amounts of carbonate-rich melts would be required to produce the LW series (a quarter of xenoliths at Tok). No carbonatites have been reported at the surface in the Tok region and no carbonates have been found in Tok xenoliths so far. By contrast, Ol–Cpx cumulates and composite peridotite xenoliths with veins produced by magmas saturated in Ol and Cpx are common at the Tok site. Precipitation of metasomatic Cpx in an LW series peridotite in contact with such a vein (Fig. 3) provides unambiguous direct evidence on the nature of the metasomatic melts.

Addressing possible origins for such melts is beyond the scope of this paper. We note, however, that the presence of the Ol–Cpx cumulate and composite xenoliths at the Tok site indicates that mantle-derived magmas pooled and fractionated in the lithospheric mantle beneath Tok. Fractional crystallization of those magmas could produce a range of Mg# in residual liquids.

Evidence for multiple or multi-stage metasomatic events

Several LH series xenoliths plot between the fields of residual mantle peridotites (represented by experimental results) and those of the LW series in Figs. 4, 5, 6, 7 and 8. For example, LH lherzolites 9505-3 and 9510-16 have high CaO/Al_2O_3 (1.3–1.6) and contain metasomatic Cpx (Ionov et al. 2005b; Figs. 4a–c, 6b). Some of those LH xenoliths have chemically heterogeneous coarse olivine (likely to be enriched in Fe and Mn) and also plot on the extensions of chemical trends defined by the LW series rocks (e.g. Fe-enriched 9502-6 and 9510-16; Fig. 5b). However, those minor enrichments in the LH series are not always related to each other in the same manner as those in the LW series, e.g. the Fe-rich sample 9502-6 has low modal Cpx while the Cpx-rich xenolith 9505-3 has high $Mg\#_{Ol}$. Most importantly, none of those LH series rocks shows low SiO_2 on the SiO_2-MgO plot (Fig. 5a), which is a distinctive feature of the LW series. Hence, the enrichments in Fe, Mn, Ti and modal Cpx observed in some LH series peridotites may not indicate the early stages of the formation of the LW series, but could rather be caused by entrapment of small-volume basaltic or carbonate-rich (for rocks with high Ca/Al) melts. It is possible that the transformation of LH series protoliths into LW series rocks requires not only appropriate melt compositions, but also that a threshold temperature or melt fraction be achieved before significant melt percolation and hence reaction could take place. The clear distinction between the olivine from the LW and LH series rocks on Mg#–Mn–Ni diagrams (Fig. 9) could be produced if the peridotite–melt (olivine–melt) re-equilibration takes place rapidly after a critical melt fraction, and hence sufficient rock permeability (Zhu and Hirth 2003), is achieved.

While formation of metasomatic Cpx and Fe-enrichments in the LW series must be related to interaction with migrating silicate melts, the combination of high Na and Cr contents in the Cpx (Fig. 12) is unlikely to be a result of equilibration with any common mantle magma. This was earlier demonstrated for LH series Cpx using comparisons with Cpx micro-phenocrysts in Na-rich glass in mantle xenoliths (Ionov et al. 2005b). Here, we show also that cumulate Cpx in xenolith 9508-14 (which crystallised from evolved magma) has lower Na (and Cr) contents than Cpx in any LW series xenolith (Fig. 12). Furthermore, Na in the Cpx is not correlated with Fe (or Ti), i.e. the Na-rich Cpx usually are

not enriched in Fe. Hence, the Na-enrichments in the Cpx (as well as high K in bulk rocks, Fig. 8b) require either entrapment of residual melts when the melt percolation comes to an end or, most likely, a separate late-stage enrichment event by alkali-rich fluids. Overall, the metasomatism was a complex process and possibly involved several stages and different (or evolving) melt/fluid compositions.

Nevertheless, the replacement of Opx by Cpx and Fe-enrichments by reactive melt percolation constituted by far the most important metasomatic event (in terms of the magnitude of modal and chemical changes), ultimately responsible for the formation of the LW series rocks. It is possible that the local entrapment of the late-stage residual melts at the end of that process resulted in small-scale precipitation of volatile-bearing accessory minerals, like amphibole, phlogopite or phosphates. The LW series rocks also bear evidence for interaction with late-stage, alkali-rich fluids, which may not have been directly related to the earlier melt percolation event. Importantly, those late-stage metasomatic phenomena are also widespread in the refractory LH series rocks (even though they may differ in details) and hence are not specific to the LW series and not directly relevant to its formation. Some of those small-scale metasomatic events, like precipitation of interstitial feldspar and spongy Cpx, probably took place only shortly before the transport of the xenoliths to the surface. In the following section, we focus on the principal melt percolation event that produced the Tok LW series.

Mg# modelling in TOK peridotites

Whole-rock Mg# and modal Cpx/Opx in LH series and LW series peridotites are negatively correlated (Fig. 14). As discussed earlier, we interpret this general correlation as an indication that the LW series rocks may have been enriched in iron as a result of a melt infiltration event, which also caused reactive Cpx enrichment. Modal variations in the Tok peridotites (Fig. 4) are consistent with the hypothesis that Cpx crystallization was accompanied by dissolution of Opx and possibly minor precipitation of olivine. In addition, the Cpx-forming reaction probably involved melt consumption because it caused "re-fertilization" of the peridotite protolith (enrichments in Ca, Fe, Al, Na and Ti; Figs. 5, 6, 7, 8). In principle, the peridotite–melt reaction at decreasing melt mass—also referred to as "percolative fractional crystallization" by Harte et al. (1993)—should decrease Mg# in percolating melt (due to olivine and Cpx crystallization), and therefore in host peridotites. However, significant Mg# variations in peridotite–melt systems are hampered by the buffering effect of Mg-rich olivine, whose mass in the peridotite matrix greatly exceeds that of interstitial melt. To evaluate the effects of the reaction and peridotite re-equilibration with infiltrated melt, we performed numerical simulations of Cpx-forming reactive melt infiltration with the "Plate Model" of Vernières et al. (1997) modified for Mg# modelling. A detailed description of the modelling procedure is provided in the Electronic Supplementary Material.

As discussed by Hanson and Langmuir (1978), Mg and Fe can be considered as trace elements during melt–rock interaction processes. Hence, a "K_d approach" can be applied to the modelling as long as the stoichiometry of the solid phases is respected (e.g. the sum MgO + FeO in olivine must be kept constant at 66.67 mol%). In turn, the mineral stoichiometry imposes strong limitations on the extent of Mg–Fe exchange between solid and liquid phases. To avoid the stoichiometry violation, we used a total inverse method (Tarantola and Valette 1982) to constrain Mg–Fe redistribution between solid and liquid phases after each reaction increment. Another change in the "Plate Model" required by Mg–Fe modelling was to allow variations of Mg and Fe olivine/melt K_d values during the experiments as a function of the Mg and Fe contents in percolating melt, based on the experimental constraints (Ulmer 1989).

For modelling, the Cpx-forming reaction takes the general form:

$$(1 + 100f)\mathrm{liq}_0 + q_{\mathrm{opx}}\mathrm{opx} \rightarrow (100f)\ \mathrm{liq}_r + q_{\mathrm{cpx}}\mathrm{cpx} + q_{\mathrm{ol}}\mathrm{olivine} \quad (1)$$

where liq_0 and liq_r represent the infiltrated and residual ("reacted") melts, respectively, f is the mass fraction of residual melt after each reaction increment (with $0 < f < 1$), and q_{ol}, q_{opx} and q_{cpx} are crystallised/dissolved mass fractions of olivine, Opx and Cpx during the reaction (with $q_{\mathrm{ol}} + q_{\mathrm{opx}} + q_{\mathrm{cpx}} = 1$) (Vernières et al. 1997). Spinel was not considered in the modelling because of its low abundances in peridotites and thus little effect on whole-rock Mg#. The results shown in Fig. 14 were calculated with f arbitrarily fixed at 0.99 (i.e. each reaction step involved 1% crystallization of the melt fraction). We made sure that similar results could be obtained with different f values, provided that the number of increments is adjusted to achieve similar melt/rock ratios and reaction degrees. Our constraints on q_{ol}, q_{opx} and q_{cpx} values were twofold: (1) reproducing the lherzolite to wehrlite modal variations observed in the LW series, and (2) covering a wide range of values (0.02–0.3) for the R parameter, which stands for the mass ratio of crystallised minerals to infiltrated melt:

$$R = q_{\mathrm{cpx}} + q_{\mathrm{ol}}/(1 + 100f) \quad (2)$$

The results shown in Fig. 14 indicate that the reaction alone (involving a melt in equilibrium with host peridotite with regard to Mg and Fe, i.e. Mg# = 0.91 in the peridotite; Mg# = 0.76 in melt) produces only minor Mg# variations in the range 0.90–0.91. Hence "modal re-fertilization" (i.e. partial crystallization of infiltrated melt) cannot account for the low Mg# in the LW series and even in some LH series xenoliths.

A second set of numerical modelling involves infiltration of a melt with Mg# of 0.63, like that in the host

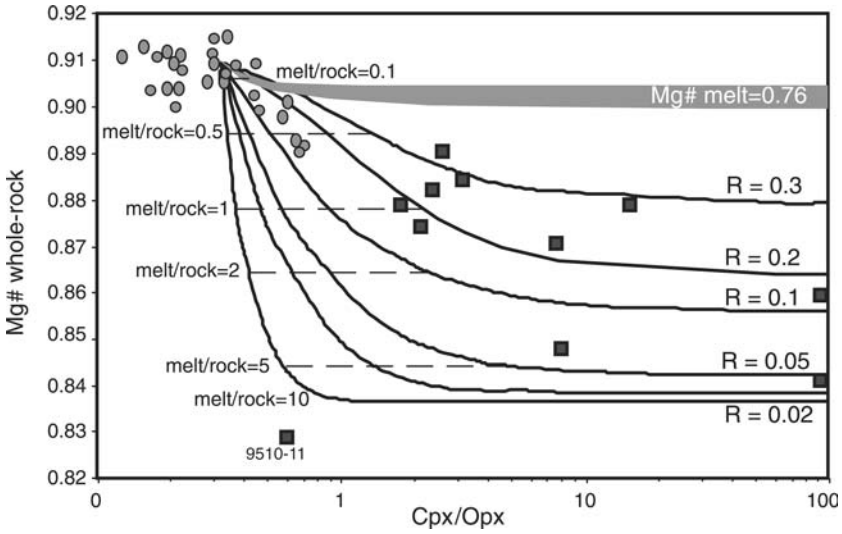

Fig. 14 A plot of whole-rock Mg# vs. modal Cpx/Opx (wt %) in Tok peridotites compared with results of numerical modelling of Mg# variations produced by interaction of a refractory peridotite (Mg# = 0.91; Cpx/Opx = 0.32) with percolating basaltic liquids involving Cpx-forming reactions at decreasing melt mass. The modelling was done using the "Plate Model" of Vernières et al. (1997) initially designed for trace-element applications and modified here for Mg–Fe modelling (see text and the electronic supplementary material). Olivine/melt and inter-mineral K_d values for Mg and Fe were fixed for T = 1,200°C and P = 1.5 GPa from experimental calibrations (Brey and Köhler 1990; Ulmer 1989). Furthermore, the olivine/melt K_d are adjusted as a function of melt composition. The initial peridotite composition (protolith) was obtained by averaging compositions of LH series rocks [with Mg# >0.90 to avoid samples possibly affected by small degrees of melt–rock reaction (Ionov et al. 2005b)]. Numerical experiments were performed with two extreme compositions for infiltrated melt: (1) a primitive, high-Mg# (0.76) liquid in equilibrium with the protolith and (2) an evolved, low Mg# (0.63) liquid similar to the host basalt. All modelling results obtained with the primitive melt composition plot in the shaded area. Modelling results for the evolved melt composition are shown for R values (mass ratio of crystallised minerals to infiltrated melt) ranging from 0.02 to 0.3. Based on Eq. 1 in text and constant f (residual melt fraction) = 0.99, the melt–host reaction parameters range from [0.99 liq_0 + 0.01 opx → 0.98 liq_r + 0.01782 cpx + 0.00198 ol] for R = 0.02 to [0.769 liq_0 + 0.231 opx → 0.761 liq_r + 0.215 cpx + 0.023 ol] for R = 0.3

basalt (Table 2), that is much lower than required by equilibrium with the initial peridotite host (Mg# = 0.76). Variation of Mg# in the interstitial melt as a function of the melt/rock ratio is shown in Fig. 15. For simplicity, and because the Cpx-forming reaction produces only minor Mg# variations (see earlier text), this experiment was run without reaction. Figure 15 indicates that the buffering of Mg–Fe in the melt by the host peridotite is effective even at high melt–rock ratios; only for melt/rock ratios greater than 10 the composition of the peridotite–melt system is mainly controlled by the infiltrated, "disequilibrium" melt. Olivine-rich peridotites, more refractory than the lherzolite used for modelling, would require even higher melt/rock ratios to be re-equilibrated. Nevertheless, substantial variations in the composition of melt in equilibrium with the peridotite protolith are observed at relatively low melt/rock ratios (Mg# varies from 0.76 to 0.70 for melt/rock ratios varying from 0 to 1, Fig. 15).

The results of modelling involving "disequilbrium" melt (Mg# = 0.63) match almost the whole Mg# range in the Tok xenoliths (Fig. 14). With this infiltrated melt composition, the LW series is best reproduced at R values in the range 0.05–0.3, and melt/rock ratios in the range 0.5–2 for peridotites with Mg# 0.87–0.89 and >4 for peridotites with Mg# <0.85. The very low Mg# (0.83) of LW series lherzolite 9510-11 can only be produced with a more evolved melt (Mg# <0.63). Because actual values of several parameters such as R, melt/rock ratios and Mg# in infiltrated melt are unknown, there is no unique solution to this modelling. For example, LW peridotites with Mg# ranging from 0.87 to 0.89 could be obtained with a set of parameters involving less evolved (higher Mg#) melt compositions, higher melt/rock ratios and lower R values.

Nevertheless, even with a different set of R and melt/rock values, our results imply that the infiltrated melt, which reacted with the LH-type protolith to form the LW series, was more evolved than required by equilibrium with averaged LH series rocks (Mg# = 0.76), and most likely characterised by Mg# values in the range 0.6–0.7. These low Mg# values inferred for the melt imply that the melt evolved by crystal fractionation before infiltrating the peridotite. Ol–Cpx cumulates (Figs. 2g–h, 3) in the Tok xenolith suite may be products of such fractionation. Together with the high melt/rock ratios estimated for significant peridotite re-equilibration, this strongly indicates that the LW series peridotites represent metasomatised mantle wall rocks adjacent to magma conduits or chambers. Minor enrichments in Fe and Cpx observed in some LH series peridotites can be obtained by smaller degrees of peridotite–melt

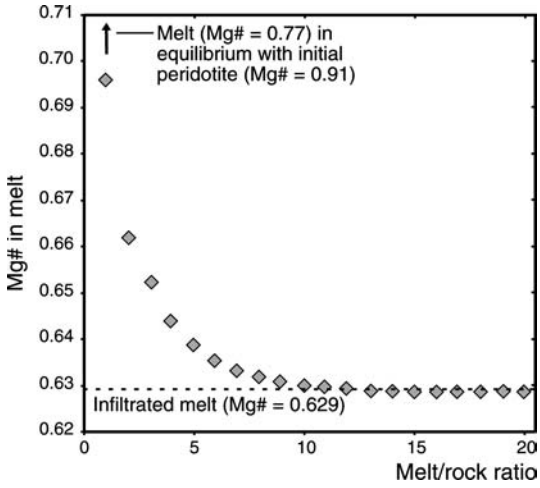

Fig. 15 Variation of Mg# in interstitial melt after infiltration of a low-Mg# (0.63) melt in a peridotite protolith (Mg# = 0.91) calculated as a function of melt/rock ratio (see text and legend of Fig. 14). The modelling was run without the Cpx-forming reaction, which produces only minor changes on this plot. Standard deviations on Mg# resulting from the total inversion applied after each melt addition increment (higher melt/rock) are smaller than the size of the symbols

interaction processes. Such rocks were probably located at greater distances from large magmatic chambers or made up wall rocks of small and short-living conduits.

Wehrlites and Fe-enriched lherzolites in the lithospheric mantle

Collectively, the petrographic, modal and chemical data on the Tok xenoliths, as well as the modelling results, indicate that the LW series rocks were formed by profound transformation of refractory residual peridotites, which experienced percolation and fractional crystallization of evolved silica-undersaturated silicate liquids. The peridotite–melt interaction produced a range of Fe-enrichments and reactive replacement of Opx by Cpx. The main event was followed by local entrapment of migrating residual melts and also by interaction with late-stage fluids enriched in alkalies and phosphorus.

The theoretical modelling in this study has highlighted several essential aspects of the melt percolation event. In particular, the melts must be evolved, Fe-rich silicate liquids rather then primary, Mg-rich magmas equilibrated with fertile or refractory mantle. The hypothetical liquids responsible for the metasomatism may have been related to melts that produced Ol–Cpx cumulate Tok xenoliths, but were not necessarily identical to the latter and probably had a range of compositions. For example, Cpx from strongly metasomatised LH series xenoliths have a broad range of Hf–Nd–Sr isotope compositions, in particular some of them have lower $^{143}Nd/^{144}Nd$ than cumulate 9508-14 and the host basalt (Ionov et al. 2001, D.A. Ionov et al. submitted for publication).

The formation of the LW series must have been a large-scale event that affected a large portion of the continental lithospheric mantle (CLM) beneath Tok in the depth range 40–60 km and possibly deeper. Because about a quarter (12/44) of all Tok xenoliths, for which chemical data are available, are grouped with the LW series, such rocks must be fairly abundant in the CLM. Moreover, some LH series xenoliths show minor effects of melt metasomatism as well. Overall, this requires large quantities of mantle-derived melts and hence an important thermal anomaly in the deeper mantle. It is possible that the melts pooled in the CLM rather than escaping to the surface because of relatively large thickness of the initial ancient cratonic CLM. The Tok peridotite suite arguably provides some of the strongest cases of the transformation of the CLM by percolating magmas, possibly because of its position near the margin of the craton affected by subduction in the Pacific and other large-scale tectono-magmatic events in eastern Asia in the Mesozoic and Cenozoic. Some analogies could possibly be drawn between these processes in the CLM at the SE Siberian craton and large-scale delamination of ancient cratonic mantle inferred for some portions of the North China craton in the Phanerozoic (e.g. Menzies et al. 1993; Xu et al. 2003).

Another example of a cratonic CLM domain with a large proportion of Fe-rich peridotites is northern Tanzania, where about 75% of xenolith population at the Labait volcano are reported to be Fe-rich (Mg# <0.88) while the rest are mainly refractory residual peridotites (Lee and Rudnick 1999). As discussed by Lee and Rudnick (1999), the large-scale Fe-enrichments and heating in the CLM must have important geophysical consequences, like increased density and lower buoyancy and seismic velocities. It is also likely that the magmatic event resulted in significant erosion and delamination of the deeper ancient CLM in the Tok area, assisted by a density increase due to Fe-enrichment. The Tok LW series rocks also have much in common with xenoliths from ocean islands (Grégoire et al. 2000; Hauri and Hart 1994; Neumann et al. 2002; Tommasi et al. 2004) representing deeply metasomatised lithospheric "lids" above hot spots.

As discussed earlier, precipitation of metasomatic Cpx in mantle peridotites and formation of wehrlites has been attributed by some workers to infiltration of carbonate-rich melts (e.g. Hauri et al. 1993; Yaxley et al. 1991). Moreover, the replacement of Opx by Cpx and the presence of apatite in various peridotites, as well as the presence of LW series rocks in xenolith suites, were postulated to be distinctive features of "carbonatite" mantle metasomatism (see Laurora et al. (2001) and Ionov et al. (2002) for reviews). All Tok LW series xenoliths show widespread replacement of Opx by Cpx or are pure wehrlites, and all of them contain apatite (Table 1). A major conclusion of this study is that those features can be produced by percolation of evolved silicate melts and hence cannot be considered as unambiguous indices of "carbonatite" metasomatism. We do not rule out,

however, that small-scale infiltration of carbonate-rich fluids is responsible for metasomatic Cpx and high Ca/Al in some LH series Tok xenoliths. Moreover, such processes probably took place after the main melt percolation event that produced the LW series rocks and could be responsible for late-stage precipitation of interstitial phosphates, and possibly Na-enrichments in the Cpx, in the LH and LW series Tok xenoliths. It is certain, however, that they cannot be the major reason for the formation of the Fe-rich lherzolites and wehrlites.

Summary of conclusions

1. About a quarter of peridotite xenoliths at the Tok volcanic field in the SE Siberian craton are grouped as LW series characterised by low Mg# (<0.89), complete or partial replacement of Opx by Cpx and high modal Cpx/Opx.
2. Based on petrographic and chemical data, the LW series was produced by metasomatic transformation of refractory residual peridotites akin to the LH series Tok xenoliths. We use theoretical modelling to argue that the most important part of that process was reactive percolation of evolved, silica-undersaturated silicate melts, most likely, in the vicinity of magma chambers and conduits. It was followed by small-scale, localised fluid-related metasomatism to produce enrichments in alkalies and phosphorus.
3. Replacement of Opx by Cpx and the presence of apatite in mantle peridotites alone cannot be considered unambiguous indices of "carbonatite" metasomatism and should be supplemented by evidence that apatite and Cpx are cogenetic as well as trace element and other relevant data. High modal Cpx in combination with low Mg# are more likely to be produced by reaction with evolved nepheline–normative silicate melts.

Acknowledgements DAI thanks V. Prikhodko for help with fieldwork and acknowledges financial, analytical and other contributions from S. Shirey, D. Weis, A. Hofmann, G. Brey, A. Sobolev, E. Takazawa, D. Kuzmin, C. Merlet, G. Chazot, M. Veschambre, S. Portales. Reviews by M. Seyler, M. Grégoire and G. Sühr and editorial comments of J. Hoefs helped to improve the paper and are highly appreciated. The fieldwork at Tok was organised by ITIG, Far Eastern Branch of Russian Academy of Sciences. Some funding and assistance were provided by Australian Research Council, DTM-CIW (Washington, DC, USA), Université Blaise Pascal at Clermont-Ferrand (France) and Belgian FNRS.

References

Batanova VG, Suhr G, Sobolev AV (1998) Origin of geochemical heterogeneity in the mantle peridotites from the Bay of Islands ophiolite, Newfoundland, Canada: ion probe study of clinopyroxenes. Geochim Cosmochim Acta 62:853–866

Bodinier J-L, Godard M (2003) Orogenic, ophiolitic and abyssal peridotites. In: Carlson RW (ed) Treatise on geochemistry, vol. 2. The mantle and core. Elsevier, Amsterdam, pp 103–170

Boyd FR, Pearson DG, Nixon PH, Mertzman SA (1993) Low-calcium garnet harzburgites from southern Africa: their relations to craton structure and diamond crystallisation. Contrib Mineral Petrol 113:352–366

Boyd FR, Pokhilenko NP, Pearson DG, Mertzman SA, Sobolev NV, Finger LW (1997) Composition of the Siberian cratonic mantle: evidence from Udachnaya peridotite xenoliths. Contrib Mineral Petrol 128:228–246

Brey GP, Köhler T (1990) Geothermobarometry in four-phase lherzolites II. New thermobarometers, and practical assessment of existing thermobarometers. J Petrol 31:1353–1378

Dalton JA, Wood BJ (1993) The compositions of primary carbonate melts and their evolution through wallrock reaction in the mantle. Earth Planet Sci Lett 119:511–525

Faul UH (1997) Permeability of partially molten upper mantle rocks from experiments and percolation theory. J Geophys Res 102:10299–10311

Fodor RV, Galar P (1997) A view into the subsurface of Mauna Kea volcano, Hawaii: crystallization processes interpreted through the petrology and petrography of gabbroic and ultramafic xenoliths. J Petrol 38:581–624

Frey FA, Green DH (1974) The mineralogy, geochemistry and origin of lherzolite inclusions in Victorian basanites. Geochim Cosmochim Acta 38:1023–1059

Frey FA, Prinz M (1978) Ultramafic inclusions from San Carlos, Arizona: petrologic and geochemical data bearing on their petrogenesis. Earth Planet Sci Lett 38:129–176

Godard M, Jousselin D, Bodinier J-L (2000) Relationships between geochemistry and structure beneath a palaeo-spreading centre: a study of the mantle section in the Oman ophiolite. Earth Planet Sci Lett 180:133–148

Grégoire M, Moine BN, O'Reilly SY, Cottin JY, Giret A (2000) Trace element residence and partitioning in mantle xenoliths metasomatised by highly alkaline, silicate- and carbonate-rich melts (Kerguelen Islands, Indian Ocean). J Petrol 41:477–509

Hanson GN, Langmuir CH (1978) Modelling of major elements in mantle–melt systems using trace element approaches. Geochim Cosmochim Acta 42:725–742

Harte B, Hunter RH, Kinny PD (1993) Melt geometry, movement and crystallization, in relation to mantle dykes, veins and metasomatism. Phil Trans R Soc London A 342:1–21

Hauri EH, Hart SR (1994) Constraints on melt migration from mantle plumes: A trace element study of peridotite xenoliths from Savai'i, Western Samoa. J Geophys Res 99:24301–24321

Hauri EH, Shimizu N, Dieu JJ, Hart SR (1993) Evidence for hotspot-related carbonatite metasomatism in the oceanic upper mantle. Nature 365:221–227

Hellebrand E, Snow JE, Hoppe P, Hofmann AW (2002) Garnet-field melting and late-stage refertilization in 'residual' abyssal peridotites from the Central Indian Ridge. J Petrol 43:2305–2338

Hofmann AW (1988) Chemical differentiation of the Earth: the relationship between mantle, continental crust, and oceanic crust. Earth Planet Sci Lett 90:297–314

Ionov DA, Savoyant L, Dupuy C (1992) Application of the ICP-MS technique to trace element analysis of peridotites and their minerals. Geostand Newsl 16:311–315

Ionov DA, Grégoire M, Prikhod'ko VS (1999) Feldspar–Ti-oxide metasomatism in off-cratonic continental and oceanic upper mantle. Earth Planet Sci Lett 165:37–44

Ionov D, Weis D, Shirey S, Prikhod'ko V, Chazot G (2001) Trace element and Os–Hf–Nd–Sr isotope systematics of pervasively metasomatised ancient lithospheric mantle at the southeastern rim of the Siberian craton. Eos Trans AGU, Fall Meet Suppl 82(47):V52B-01 (Abstract)

Ionov DA, Bodinier J-L, Mukasa SB, Zanetti A (2002) Mechanisms and sources of mantle metasomatism: major and trace element compositions of peridotite xenoliths from Spitsbergen in the context of numerical modeling. J Petrol 43:2219–2259

Ionov DA, Ashchepkov I, Jagoutz E (2005a) The provenance of fertile off-craton lithospheric mantle: Sr–Nd isotope and chemical composition of garnet and spinel peridotite xenoliths from Vitim, Siberia. Chem Geol 217:41–75

Ionov DA, Prikhodko VS, Bodinier J-L, Sobolev AV, Weis D (2005b) Lithospheric mantle beneath the south-eastern Siberian craton: petrology of peridotite xenoliths in basalts from the Tokinsky Stanovik. Contrib Mineral Petrol (in press)

Jackson ED, Wright TL (1970) Xenoliths in the Honolulu volcanic series, Hawaii. J Petrol 11:405

Kalfoun F, Ionov D, Merlet C (2002) HFSE residence and Nb–Ta ratios in metasomatised, rutile-bearing mantle peridotites. Earth Planet Sci Lett 199:49–65

Kelemen PB, Dick HJ, Quick JE (1992) Formation of harzburgite by pervasive melt/rock reaction in the upper mantle. Nature 358:635–641

Kiselev AI, Medvedev ME, Golovko GA (1979) Volcanism of the Baikal rift zone and problems of deep magma generation. Nauka, Novosibirsk, p 197 (in Russian)

Laurora A, Mazzucchelli M, Rivalenti G, Vannucci R, Zanetti A, Barbieri MA, Cingolani CA (2001) Metasomatism and melting in carbonated peridotite xenoliths from the mantle wedge: the Gobernador Gregores case (southern Patagonia). J Petrol 42:69–87

Lee C-T, Rudnick RL (1999) Compositionally stratified cratonic lithosphere: petrology and geochemistry of peridotite xenoliths the Labait volcano, Tanzania. In: Gurney JJ, Gurney JL, Pascoe MD et al (eds) Proc 7th Internatl Kimberlite Conf, vol 1. RedRoof Design, Cape Town, pp 503–521

Liu X, O'Neill HSC (2004) The effect of Cr_2O_3 on the partial melting of spinel lherzolite in the system CaO–MgO–Al_2O_3–SiO_2–Cr_2O_3 at 1.1 GPa. J Petrol 45:2261–2286

Menzies MA, Hawkesworth CJ (1987) Mantle metasomatism. Academic, London, pp 500

Menzies MA, Fan W, Zhang M (1993) Paleozoic and Cenozoic lithoprobes and the loss of >120 km of Archaean lithosphere, Sino-Korean craton. Geol Soc London Spec Publ 76:71–81

Neumann E-R, Wulff-Pedersen E, Pearson NJ, Spenser EA (2002) Mantle xenoliths from Tenerife (Canary Islands): evidence for reactions between mantle peridotites and silicic carbonatite melts inducing Ca metasomatism. J Petrol 43:825–857

Niu Y (1997) Mantle melting and melt extraction processes beneath ocean ridges: evidence from abyssal peridotites. J Petrol 38:1047–1074

Parkinson IJ, Arculus RJ, Eggins SM (2003) Peridotite xenoliths from Grenada, Lesser Antilles Island Arc. Contrib Mineral Petrol 146:241–262

Pearson DG, Canil D, Shirey SB (2003) Mantle samples included in volcanic rocks: xenoliths and diamonds. In: Carlson RW (ed) Treatise on geochemistry, vol 2. The mantle and core. Elsevier, Amsterdam, pp 171–276

Peslier AH, Francis D, Ludden J (2002) The lithospheric mantle beneath continental margins: melting and melt–rock reaction in Canadian Cordillera xenoliths. J Petrol 43:2013–2047

Press S, Witt G, Seck HA, Ionov DA, Kovalenko VI (1986) Spinel peridotite xenoliths from the Tariat Depression, Mongolia. I: Major element chemistry and mineralogy of a primitive mantle xenolith suite. Geochim Cosmochim Acta 50:2587–2599

Rasskazov SV, Boven A, Ivanov AV, Semenova VG (2000) Middle Quaternary volcanic impulse in the Olekma-Stanovoy mobile system: 40Ar–39Ar dating of volcanics from the Tokinsky Stanovik (in Russian). Tikhookeanskaya Geologiya 19:19–28

Semenova VG, Solovyeva LV, Vladimirov BM (1984) Deep-seated inclusions in alkali basaltoids of the Tokinsky Stanovik (in Russian). Nauka, Novosibirsk, p 119

Shirey SB, Walker RJ (1998) The Re–Os isotope system in cosmochemistry and high-temperature geochemistry. Ann Rev Earth Planet Sci 26:423–500

Smith D (2000) Insights into the evolution of the uppermost continental mantle from xenolith localities on and near the Colorado Plateau and regional comparisons. J Geophys Res 105:16769–16781

Streckeisen A (1976) To each plutonic rock its proper name. Earth Sci Rev 12:1–33

Takazawa E, Frey FA, Shimizu N, Obata M (2000) Whole rock compositional variations in an upper mantle peridotite (Horoman, Hokkaido, Japan): are they consistent with a partial melting process. Geochim Cosmochim Acta 64:695–716

Takazawa E, Okayasu T, Satoh K (2003) Geochemistry and origin of the basal lherzolites from the northern Oman ophiolite (northern Fizh block). Geochem Geophys Geosyst 4. DOI 10.1029/2001GC000232

Tarantola A, Valette B (1982) Generalized non-linear inverse problems solved using least-squares criterion. Rev Geophys Space Phys 20:219–232

Tommasi A, Godard M, Coromina G, Dautria J-M, Barsczus H (2004) Seismic anisotropy and compositionally induced velocity anomalies in the lithosphere above mantle plumes: a petrological and microstructural study of mantle xenoliths from French Polynesia. Earth Planet Sci Lett 227:539–556

Toramaru A, Fujii N (1986) Connectivity of melt phase in a partially molten peridotite. J Geophys Res 91:9239–9252

Ulmer P (1989) The dependence of the Fe^{2+}–Mg cation-partitioning between olivine and basaltic liquid on pressure, temperature and composition: an experimental study to 30 kbar. Contrib Mineral Petrol 101:261–273

Vernières J, Godard M, Bodinier J-L (1997) A plate model for the simulation of trace element fractionation during partial melting and magma transport in the Earth's upper mantle. J Geophys Res 102:24771–24784

Walter MJ (2003) Melt extraction and compositional variability in mantle lithosphere. In: Carlson RW (ed) Treatise on geochemistry, vol 2. The mantle and core. Elsevier, Amsterdam, pp 363–394

Wiechert U, Ionov DA, Wedepohl KH (1997) Spinel peridotite xenoliths from the Atsagin-Dush volcano, Dariganga lava plateau, Mongolia: a record of partial melting and cryptic metasomatism in the upper mantle. Contrib Mineral Petrol 126:345–364

Wilshire HG, Shervais JW (1975) Al-augite and Cr-diopside ultramafic xenoliths in basaltic rocks from western United States. Phys Chem Earth 9:257–272

Xu YG, Mercier J-CC, Menzies MA, Ross JV, Harte B, Lin C, Shi L (1996) K-rich glass-bearing wehrlite xenoliths from Yitong, northeastern China: petrological and chemical evidence for mantle metasomatism. Contrib Mineral Petrol 125:406–420

Xu Y-G, Menzies MA, Thirlwall MF, Huang X-L, Liu Y, Chen X-M (2003) 'Reactive' harzburgites from Huinan, NE China: products of the lithosphere–asthenosphere interaction during lithospheric thinning? Geochim Cosmochim Acta 67:487–505

Yaxley GM, Crawford AJ, Green DH (1991) Evidence for carbonatite metasomatism in spinel peridotite xenoliths from western Victoria, Australia. Earth Planet Sci Lett 107:305–317

Zhu W, Hirth G (2003) A network model for permeability in partially molten rocks. Earth Planet Sci Lett 212:407–416

Zonenshain LP, Kuzmin MI, Natapov LM (1990) Geology of the USSR: a plate tectonic synthesis. Am Geophys Union Geodynam Ser 21:242